Lithos 125 (2011) 875–896

Contents lists available at ScienceDirect

Lithos

journal homepage: www.elsevier.com/locate/lithos

Geochronology, geochemistry and tectonic evolution of the Western and Central cordilleras of Colombia

Diego Villagómez [a], Richard Spikings [a,*], Tomas Magna [b,e,f], Andreas Kammer [c], Wilfried Winkler [d], Alejandro Beltrán [d]

[a] Section of Earth and Environmental Sciences, University of Geneva, 13 Rue des Maraîchers, 1205 Geneva, Switzerland
[b] Institut für Mineralogie, Westfälische Wilhelms-Universität Münster, Corrensstrasse 24, D-48149 Münster, Germany
[c] Departamento de Geociencias, Universidad Nacional de Colombia, A.A. 14490 Bogotá, Colombia
[d] Geologisches Institut, ETH-Zürich, 8092 Zürich, Switzerland
[e] Institute of Mineralogy and Geochemistry, University of Lausanne, CH-1015 Lausanne, Switzerland
[f] Czech Geological Survey, Klarov 3, CZ-118 21 Prague, Czech Republic

ARTICLE INFO

Article history:
Received 11 March 2011
Accepted 6 May 2011
Available online 15 May 2011

Keywords:
Geochronology
Geochemistry
Tectonics
Central Cordillera Colombia
Western Cordillera Colombia

ABSTRACT

Autochthonous rocks of the pre-Cretaceous continental margin of NW South America (the Tahami Terrane) are juxtaposed against a series of para-autochthonous rock units that assembled during the Early Cretaceous. Allochthonous, oceanic crust of the Caribbean Large Igneous Province collided with and accreted onto the margin during the Late Cretaceous. We present the first regional-scale dataset of zircon U–Pb LA–ICP–MS ages for intrusive and metamorphic rocks of the autochthonous Tahami Terrane, Early Cretaceous igneous para-autochthonous rocks and accreted oceanic crust. The U–Pb zircon data are complemented by multiphase $^{40}Ar/^{39}Ar$ crystallization and cooling ages. The geochronological data are combined with whole rock major oxide, trace element and REE data acquired from the same units to constrain the tectonic origin of the rock units and terranes exposed in the Western Cordillera, Cauca–Patía Valley and the Central Cordillera of Colombia. The Tahami Terrane includes lower Paleozoic orthogneisses (~440 Ma) that may have erupted during the active margin stage of the Rheic Ocean. Basement gneisses were intruded by Permian, continental arc granites during the final assembly of Pangea. Triassic sedimentary rocks were subsequently deposited in rift basins and partially melted during high-T metamorphism associated with rifting of western Pangea during 240–220 Ma. Continental arc magmatism during 180–145 Ma is preserved along the whole length of the Central Cordillera and was followed by an Early Cretaceous out-board step of the arc axis and the inception of the Quebradagrande Arc that fringed the continental margin. Back-stepping of the arc axis may have been caused by the collision of buoyant seamounts, which were coeval with plateau rocks exposed in the Nicoya Peninsular of Costa Rica. Rapid westward drift of South America closed the Quebradagrande basin in the late Aptian and caused medium-high P–T metamorphic rocks of the Arquía Complex to exhume and obduct onto the continental margin. Subduction beneath hot-spot derived rocks of the Caribbean Plateau (~100–92 Ma) formed an intra-oceanic arc (~92–75 Ma), which collectively comprise the Late Cretaceous Caribbean Large Igneous Province. The remnant ocean basin located between South America and the Caribbean Large Igneous Province was partly consumed via continental subduction, forming the large Antioquia Batholith. The Caribbean Large Igneous Province collided and accreted to South America during ~75–70 Ma along the Cauca–Almaguer Fault, resulting in the cessation of both arcs and the Paleocene onset of subduction beneath the accreted oceanic crust.

1. Introduction

The continental margin of the South American Plate in Colombia has experienced at least one complete Wilson cycle since ~600 Ma with the opening and closure of the Iapetus and Rheic oceans, and it is currently undergoing the active margin stage of the Tethys–Pacific Wilson cycle. The northern Andes (north of 5°S) are unique among the Andean mountain chain within the Pacific Wilson cycle because they include Cretaceous allochthonous terranes that consist of oceanic crust, whose collision and accretion in the Early and Late Cretaceous to South America interrupted the Andean, eastern Pacific subduction system. However, few quantitative data have been published to constrain the evolution of the northwestern corner of the South American Plate during the Phanerozoic, and therefore understand better the evolution of western Pangea, and the process of growth of continental crust by the accretion of buoyant oceanic indentors. We

* Corresponding author. Tel.: +41 22 379 3176; fax: +41 22 379 3210.
E-mail addresses: diego.villagomez@gmail.com (D. Villagómez), Richard.Spikings@unige.ch (R. Spikings), tomas.magna@uni-muenster.de (T. Magna), kammer.andreas@gmail.com (A. Kammer), wilfried.winkler@erdw.ethz.ch (W. Winkler).

0024-4937/$ – see front matter © 2011 Elsevier B.V. All rights reserved.
doi:10.1016/j.lithos.2011.05.003

present an investigation of the composition and evolution of the Paleozoic–Mesozoic South American Plate margin, and the indenting allochthonous Cretaceous rocks, using geochemical characterization, U–Pb and $^{40}Ar/^{39}Ar$ geochronology.

U–Pb LA–ICP–MS zircon geochronology has been combined with $^{40}Ar/^{39}Ar$ (hornblende, biotite and plagioclase) and geochemical analyses of igneous and metasedimentary rocks along the Paleozoic–Mesozoic margin of Colombia to constrain their stratigraphic ages, and the timing of arc magmatism and crustal anatexis during high-temperature metamorphic events. Similar data have been acquired from accreted Cretaceous oceanic crust, permitting its tectonic origin to be assessed, and to establish estimates of the timing of its collision with the South American Plate. Collectively, these rocks span the termination of the Rheic Wilson cycle and the initiation and evolution of the Tethys–Pacific cycle, and provide information about i) the timing of ocean closure, ii) subsequent continent disassembly, and iii) evolution of the Pacific margin and the interaction of the Colombian margin with the Caribbean Plate.

This work is the first regional-scale study of the rocks exposed in the Central and Western cordilleras of Colombia, which attempts to combine geochemical data with interpretable geochronological data. An improved understanding of the ages and tectonic origins of the rocks with both continental and oceanic affinities will provide new information concerning the amalgamation and disassembly of western Pangea during rifting in the western Tethys, the transition from a passive to an active margin, and evolution of the active margin during the introduction of heterogeneous oceanic crust to the trench. This improved knowledge of the evolution of northwestern South America contributes to a greater understanding of the evolution of the Caribbean Plate, which was the source region for the accreted terranes during the Early and Late Cretaceous.

2. Geological framework

The northern Andes of Colombia is comprised of three sublinear topographic ridges of the Western, Central and Eastern cordilleras, which are separated by prominent topographic depressions of the Cauca–Patía and Magdalena valleys (Fig. 1).

Allochthonous, ultramafic and mafic crystalline rocks define an oceanic province, which is thought to have accreted during the Mesozoic, and defines the basement of the Western Cordillera and the Cauca–Patía Valley. The accreted rock sequence is juxtaposed against the para-autochthonous and autochthonous paleo-continental margin across the regional-scale Romeral Fault System (Fig. 1). This broad faulted zone (up to 30 km wide) corresponds to a ~2000 km long tectonic suture that extends southwards into Ecuador (Peltetec Fault; Fig. 1), and includes anastomosed zones of ultramafic and mafic rocks, high-pressure assemblages and arc related sequences that are occasionally exposed with a tectonic mélange. Within Colombia, the suture zone can be divided into three major branches (Chicangana, 2005), which are the San Jerónimo Fault, Silvia–Pijao Fault and the Cauca–Almaguer Fault (Fig. 2), which generally define the break-of-slope of the western flank of the Central Cordillera.

2.1. Continental crust of the Central Cordillera: autochthonous terranes

Autochthonous continental crust of the Central Cordillera is exposed to the east of the Romeral Fault System (the San Jerónimo Fault; Figs. 1 and 2), and west of the Otú–Pericos Fault. Restrepo and Toussaint (1988) referred to these rocks as the Tahami Terrane, which consists of Paleozoic gneisses of the Puqui and La Miel units (Ordóñez-Carmona and Pimentel, 2002) that are in unconformable contact with overlying metasedimentary and meta-igneous rocks of the undifferentiated Cajamarca Complex. Widely dispersed and variably deformed Permo-Triassic granitoids (e.g. Cediel and Cáceres, 2003; Gómez et al., 2007) formed during Permian arc magmatism that accompanied the assembly of Pangea, and anatexis during its subsequent Triassic fragmentation (Cardona et al., 2010; Vinasco et al., 2006).

More recently, Restrepo et al. (2009a) divided the Tahami Terrane into crustal blocks that were metamorphosed at different times, and amalgamated during the late Paleozoic (Cardona et al., 2006; Vinasco et al., 2006) in the wake of continental collision that formed Pangea.

The Cajamarca Complex and older sequences are intruded and contact metamorphosed by undeformed Jurassic, calc-alkaline, I-type granitoids of the Ibagué Batholith (Fig. 2; K/Ar hornblende and biotite ages of 150–140 Ma; Vesga and Barrero, 1978; Brook, 1984), which are partly overlain by contemporaneous, high-SiO_2 volcanic rocks of the Saldaña Fm. Subsequently, the Tahami Terrane in the northern Central Cordillera was intruded by the calc-alkaline, dioritic–granitic, Late Cretaceous Antioquia Batholith (88–83 Ma) (Ibañez-Mejia et al., 2007; Fig. 2A). Continental arc granites of the Paleocene Sonsón Batholith (65–55 Ma; zircon U–Pb; Ordóñez-Carmona et al., 2001) cross-cut the Antioquia Batholith.

Published K/Ar and Rb/Sr ages of metamorphic and granitic rocks of the Central Cordillera range between 343 and 57 Ma (see compilation in Aspden et al., 1987; Restrepo et al., 2009a). Most of these ages have been interpreted to record thermal events during the early Mesozoic to early Cenozoic (McCourt et al., 1984; Restrepo et al., 2009a). However, the analytical techniques do not provide parameters that can be used to constrain the time and degree of partial resetting of the Rb/Sr and K/Ar isotopic systems, and hence the geological relevance of the ages is uncertain.

2.2. Terranes within the Romeral Fault System: The Quebradagrande and Arquía complexes

The San Jerónimo Fault separates continental rocks of the Tahami Terrane from a variably deformed belt of igneous rocks and marine to terrestrial sedimentary rocks of the Quebradagrande Complex (Fig. 2A–B). Unmetamorphosed to greenschist gabbros, diorites, basalts, andesites and tuffs of the Quebradagrande Complex are covered by marine and terrestrial sedimentary rocks of the Abejorral Fm., which hosts Hauterivian to lower Albian fossils (González, 1980). The igneous rocks are considered to have formed in either a mid-oceanic ridge setting (González, 1980), an island arc (Toussaint and Restrepo, 1994) or an ensialic marginal basin (Nivia et al., 2006). The Quebradagrande Complex is in faulted contact with isolated tectonic slices of garnet-bearing amphibolites, and lawsonite-glaucophane schists of the Arquía complex across the Silvia–Pijao Fault (Fig. 2A–B). The amphibolites have yielded a K–Ar hornblende age of ~113 Ma (Restrepo and Toussaint, 1976), a hornblende, total fusion $^{40}Ar/^{39}Ar$ age of ~107 Ma (Restrepo et al., 2008), and phengite $^{40}Ar/^{39}Ar$ ages of 120–60 Ma were obtained from the blueschists by Bustamante (2008).

The origin and timing of peak metamorphism of the Arquía Complex are poorly constrained. Nivia et al. (2006) consider the medium- and high-pressure metamorphic rocks to be Neoproterozoic continental crust, based on cross-cutting field evidence that was apparently misinterpreted (Restrepo et al., 2009b). Bustamante (2008) combined geochemistry, geothermobarometry and $^{40}Ar/^{39}Ar$ analyses (phengite) to propose that i) the protolith of the blueschists was basaltic, which was metamorphosed at ~63 Ma, and ii) the protolith of the high-pressure rocks originated at a mid-ocean ridge and equilibrated with blueschist P–T conditions prior to 120 Ma.

2.3. Allochthonous rocks in the Cauca–Patía Valley

The Cauca–Patía Valley (Figs. 1 and 2) is located immediately to the west of the Cauca–Almaguer Fault and is limited to the west by the Cali–Patía Fault. Sporadically dispersed inliers (Fig. 2A–B) reveal a basement composed of basalts and gabbros of the Amaime Fm. and

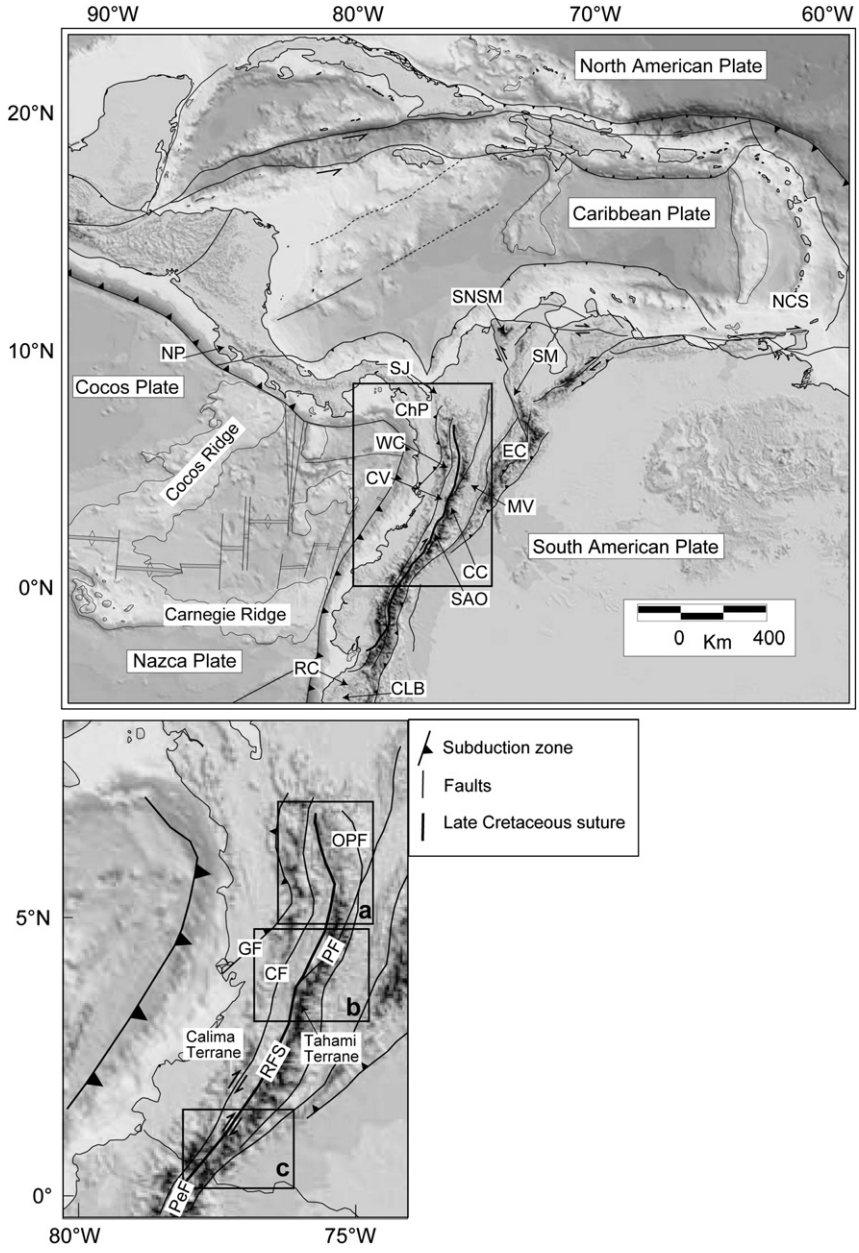

Fig. 1. Digital elevation model of northwestern South America and surrounding tectonic plates, showing the main cordilleras, faults and selected terranes (background model modified from Gómez et al. 2007). The Late Cretaceous ocean-continent suture is shown as a thick black line. Inset shows the study area in more detail, and the three regions (a, b and c) that are presented in Fig. 2. CC: Central Cordillera, CLB: Celica–Lancones Basin (Ecuador); CF: Cali–Patía Fault, CV: Cauca–Patía Valley, EC: Eastern Cordillera, GF: Garrapatas Fault, LR: La Rinconada (Margarita Island), MA: Mérida Andes; MV: Magdalena Valley, NCS: North Coast Schist (Tobago), OPF: Otú–Pericos Fault, ChP: Chocó–Panamá Block, PeF: Peltetec Fault (Ecuador), PF: Palestina Fault, RC: Raspas Complex (Amotape Province in Ecuador), RFS: Romeral Fault System, SAO: San Antonio Ophiolite Complex, SJ: San Jacinto belt, SM: Santander Massif, SNSM: Sierra Nevada de Santa Marta, WC: Western Cordillera.

ultramafic cumulate rocks of the Ginebra and Los Azules Fms. These rocks correspond with the strongly positive Bouguer gravity anomaly observed from the valley (+135 to +75 mgal; Case et al., 1971).

Aspden et al. (1987) suggested that the basement of the Cauca–Patía Valley is composed of a Jurassic–Lower Cretaceous ophiolitic sequence. However, Kerr et al. (1997) showed that these rocks formed in an oceanic plateau setting, and proposed that they may be equivalent to rocks exposed within the Western Cordillera. However, few radiometric ages have been published for the Amaime and Los Azules Fms, and include a groundmass, total fusion $^{40}Ar/^{39}Ar$ age of 76.3 ± 1.7 Ma (Sinton et al., 1998) and K/Ar ages that range between 104 and 78 Ma (De Souza et al., 1984) with potentially disturbed isotopic systems and (partially) reset ages. The Buga Batholith (Fig. 2B) intrudes the Amaime Fm., although previous Rb/Sr and K/Ar radiometric ages of 114–94 Ma (Brook, 1984) are associated with large uncertainties and do not precisely or accurately constrain the age of the intrusion.

2.4. Allochthonous rocks in the Western Cordillera and the coastal ranges

Restrepo and Toussaint (1988) group the mafic crystalline rocks of the Western Cordillera (south of the Garrapatas Fault; Fig. 1) into the Calima Terrane, whereas rocks exposed in the coastal ranges, to the west of the Garrapatas Fault form part of the Chocó–Panamá Terrane (Fig. 1). The Calima Terrane is composed of three Upper Cretaceous sequences of rocks, which are: i) imbricated pillowed and massive

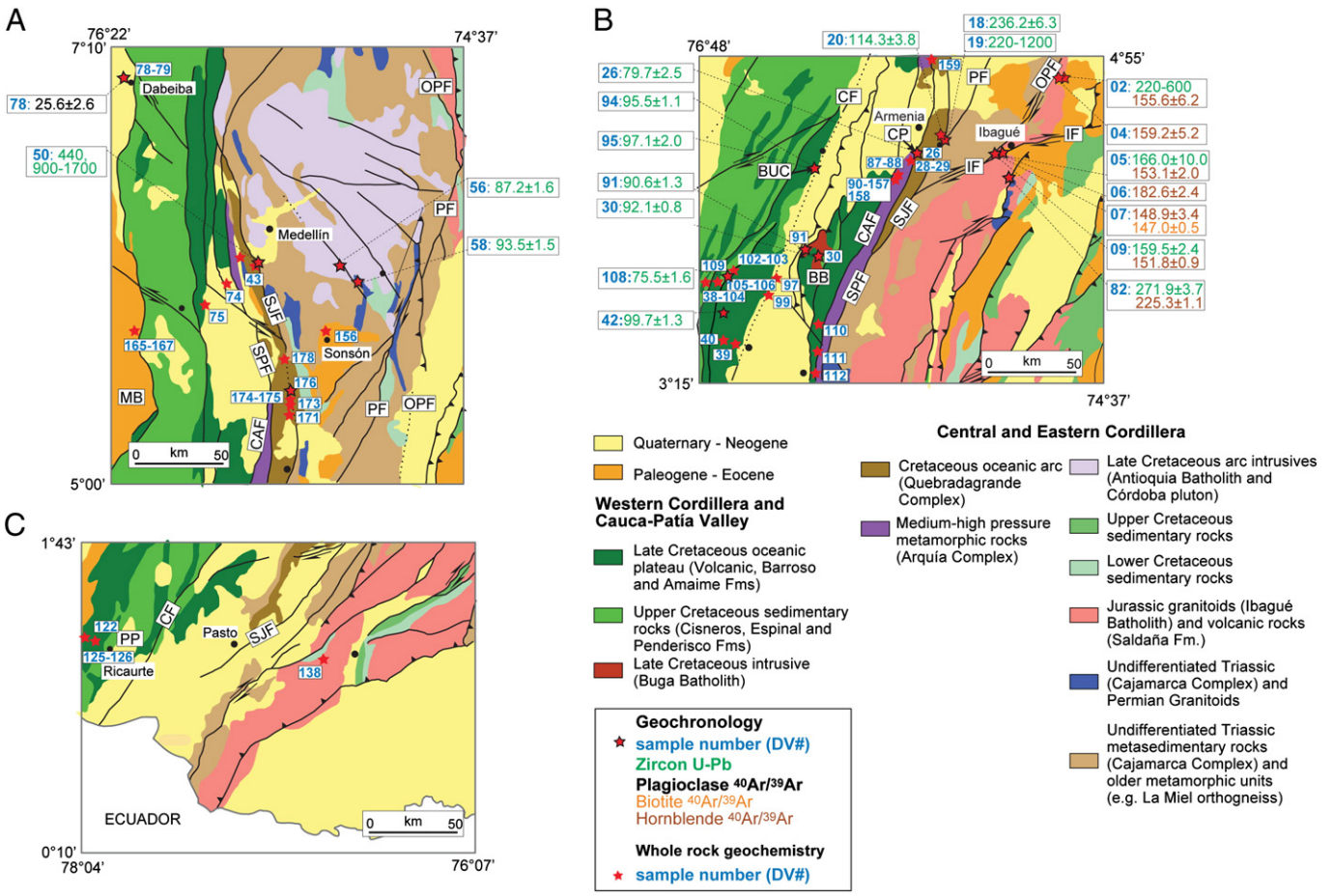

Fig. 2. Geological maps of the three study regions (see Fig. 1) within the Central and Western Cordilleras of Colombia, and the Cauca–Patía Valley (after Gómez et al., 2007), showing sample locations (sample codes shown in blue; DV#), the radiometric ages acquired in this study (±2σ error) and the locations of samples analyzed for geochemical data. (U–Pb data shown as detrital zircon peak ages for samples DV02, DV19 and DV50). All errors are reported at ±2σ. Abbreviations: Cauca–Almaguer Fault (CAF), San Jerónimo Fault (SJF) and the Silvia–Pijao Fault (SPF) collectively define the Romeral Fault System. Other abbreviations, BUC: Bolívar Ultramafic Complex (Fig. 2B), BB: Buga Batholith (Fig. 2B), CF: Cali–Patía Fault (Fig. 2C), CP: Córdoba Pluton (Fig. 2B), IF: Ibagué Fault, MB: Mande Batholith (Fig. 2A), OPF: Otú–Pericos Fault (Fig. 2B); PF: Palestina Fault (Fig. 2B), PP: Piedrancha Pluton (Fig. 2C).

basalts and gabbros of the Volcanic Fm. (Fig. 2; Barrero, 1979; Aspden, 1984; Kerr et al., 1997; Sinton et al., 1998), ii) norites, olivine norites and gabbronorites of the Bolívar Ultramafic Complex (Fig. 2B), whose incompatible trace element ratios are similar to those of the Volcanic Fm. (Kerr et al., 2004), and iii) turbidites of the Espinal and Cisneros Fms (Fig. 2), which consist of a sequence of shales with thin lenses of limestones and cherts that are occasionally slightly metamorphosed to slates and phyllites and contain Albian–Maastrichtian radiolarites and ammonites (Barrero, 1979; Etayo-Serna, 1985a). The Chocó–Panamá Terrane (Fig. 1) consists of basalt with similar geochemical characteristics to the Volcanic Fm. (Kerr et al., 1997), with groundmass and plagioclase $^{40}Ar/^{39}Ar$ ages of 78–73 Ma (Kerr et al., 1997). A single groundmass $^{40}Ar/^{39}Ar$ age of 91.7 ± 2.7 Ma has been acquired from the Volcanic Fm. (Kerr et al., 1997), which is consistent with fossil evidence obtained from intercalated sedimentary rocks. These radiometric and fossil ages are coeval with plateau rocks exposed in the Caribbean and Western Cordillera of Ecuador, most of which range between 92 and 88 Ma (Kerr et al., 1997, 1999; Luzieux et al., 2006; Sinton et al., 1997, 1998; Vallejo et al., 2009).

Consensus exists that the ultramafic and mafic rocks of the Calima and Chocó–Panamá terranes form part of the Caribbean Large Igneous Province (e.g. Kerr et al., 1997). Ultramafic to mafic rocks formed in response to Late Cretaceous, mantle plume-related volcanism in the eastern Pacific (Kerr et al., 1997; Luzieux et al., 2006; Pindell, 1990, 1993) and accreted against northwestern South America in the Campanian in Ecuador (e.g. Hughes and Pilatasig, 2002; Jaillard et al., 2004; Spikings et al., 2001, 2010; Vallejo et al., 2009). Several authors (Kerr et al., 2004; Luzieux et al., 2006; Pindell and Kennan, 2009; Sinton et al., 1998) have proposed that plateau rocks of the Caribbean Large Igneous Province erupted above the paleo-Galápagos hot spot. Spikings et al. (2001) proposed a model for northwestern South America, where the plateau fragmented into several tectonic slices during and subsequent to its collision with the northwestern margin of the South American plate.

Tertiary magmatic rocks with a subduction-related origin intrude the Calima and Chocó–Panamá terranes. The Mande Batholith (Fig. 2A; U–Pb zircon age of 43–42 Ma; Cardona, pers. comm.) and associated volcanic rocks of the Dabeiba unit (plagioclase $^{40}Ar/^{39}Ar$ 43.1 ± 0.4 Ma; Kerr et al., 1997) are exposed within the Chocó–Panamá Block in northern Colombia. Tertiary volcanic rocks of the Ricaurte Fm. are erupted onto the accreted basement of the Calima Terrane (Cediel et al., 2003), and may be correlatable with the poorly dated Macuchi Fm. in Ecuador (e.g. Vallejo et al., 2009).

3. Sampling and methods

Rocks were sampled in three distinct regions (between 7°N and 1°N; Figs. 1 and 2) that span the Central Cordillera, Cauca–Patía Valley

Table 1
Summary zircon U–Pb and $^{40}Ar/^{39}Ar$ data from the Western Cordillera, Cauca–Patía Valley and Central Cordillera of Colombia.

Sample	Stratigraphy	Lithology	Latitude deg min s	Longitude deg min s	Phase	40Ar/39Ar age ±2σ (Ma)	238U/206Pb age ±2σ (Ma)	MSWD
DV02	Cajamarca Complex	Gneiss	04 46 41.8	74 57 54.2	Zircon		238–582 (12)	
					Hornblende	155.6 ± 6.2 (p)		
DV04	Ibagué Batholith	Diorite	04 47 00.2	74 58 31.4	Hornblende	159.2 ± 5.2 (p)		
DV05	Ibagué Batholith	Granodiorite	04 24 27.7	75 16 05.3	Zircon		166.0 ± 10.0 (5)	0.29
					Hornblende	153.1 ± 2.0 (p)		
DV06	Ibagué Batholith	Granite	04 24 08.9	75 17 40.3	Hornblende	182.6 ± 2.4		
DV07	Ibagué Batholith	Granite	04 24 25.4	75 18 04.5	Hornblende	148.9 ± 3.3 (p)		
					Biotite	147.0 ± 0.5 (p)		
DV09	Ibagué Batholith	Granite	04 24 29.7	75 18 11.8	Zircon		169.6 ± 2.4 (20)	0.63
					Biotite	151.8 ± 0.9 (p)		
DV18	?	Gneiss	04 28 19.0	75 33 18.1	Zircon		236.2 ± 6.3 (13)	0.61
DV19	Cajamarca Complex	Quartzite	04 28 19.0	75 33 18.1	Zircon		231–1163 (30)	
DV20	Quebradagrande Complex	Tuff	04 29 27.8	75 34 02.0	Zircon		114.3 ± 3.8 (7)	2.00
DV26	Córdoba Pluton	Granodiorite	04 24 30.9	75 41 24.2	Zircon		79.7 ± 2.5 (13)	0.27
DV30	Buga Batholith	Granodiorite	03 54 10.6	76 10 50.4	Zircon		92.1 ± 0.8 (43)	0.66
DV42	Volcanic Fm.	Gabbro	03 37 05.0	76 39 15.1	Zircon		99.7 ± 1.3 (16)	0.62
DV50	La Miel Unit	Gneiss	06 06 15.6	75 38 02.7	Zircon		450–1811 (40)	
DV56	Antioquia Batholith	Granite	06 03 19.8	75 12 42.7	Zircon		87.2 ± 1.6 (16)	0.81
DV58	Antioquia Batholith	Granite	06 01 06.3	75 08 10.8	Zircon		93.5 ± 1.5 (14)	1.30
DV78	Dabeiba Fm.	Andesite	07 00 54.9	76 18 29.5	Plagioclase	25.6 ± 2.6 (tf)		
DV82	Permian granite	Granite	04 17 15.5	75 13 59.2	Zircon		271.9 ± 3.7 (25)	1.20
					Hornblende	225.3 ± 1.1 (tf)		
DV91	Buga Batholith	Diorite	03 55 31.0	76 14 42.4	Zircon		90.6 ± 1.3 (20)	0.38
DV94	Bolivar Ultramafic Complex	Pegmatite	04 20 25.7	76 11 44.0	Zircon		95.5 ± 1.1 (22)	0.26
DV95	Bolivar Ultramafic Complex	Pegmatite	04 20 02.1	76 11 52.0	Zircon		97.1 ± 2.0 (18)	1.20
DV108	Cisneros Fm.	Lithic Tuff	03 46 51.8	76 38 47.4	Zircon		75.5 ± 1.6 (29)	0.56

p: plateau age, tf: total fusion age.
Values in parentheses are the number of zircon grains analyzed.
MSWD values are calculated from the zircon grains that were used to calculate the 238U/206Pb age.
Raw data is presented in the online Table 5 (40Ar/39Ar) and 4 (U–Pb).

and the Western Cordillera of Colombia. Petrographic descriptions are provided in Villagómez (2010), U–Pb zircon data and $^{40}Ar/^{39}Ar$ (multi-phase) data are summarized in Table 1 and whole rock geochemical data (major oxides, trace and REE) acquired from selected samples are presented in Table 2. Raw $^{40}Ar/^{39}Ar$ and U–Pb data are presented in the online Tables 3 and 4, and the complete geochemical dataset is presented online in Table 5. Samples were crushed and milled to <300 μm and zircons, hornblende, biotite and plagioclase were extracted using conventional magnetic and density separation methods. These data are combined to constrain the tectonic origin, source regions and crystallization age of specific rock units.

3.1. Zircon U–Pb geochronology

Inclusion free zircons were handpicked for analysis and imaged by scanning electron microscope–cathodoluminescence (SEM–CL). U and Pb isotopic abundances were measured by laser-ablation inductively coupled plasma mass spectrometry (ICP–MS) analyses coupled with liquid internal Tl–U normalization, and an Excel macro, Lamdate tool (J. Košler) was used for offline data reduction together with Isoplot v. 3.31 for age calculations (Ludwig, 2003).

An Elan 6100 DRC ICP–MS (Perkin Elmer) coupled with a 193-nm Ar-F Geolas 200M Excimer-based excimer (Lambda Physik), housed at the University of Lausanne was used for U–Pb isotope analysis. Instrumental mass fractionation was corrected using a Tl–U tracer solution (natural Tl mixed with artificial ^{233}U–^{236}U; $^{236}U/^{233}U = 0.8450$ and $^{205}Tl/^{233}U = 1.2$) aspirated through an Apex desolvating nebulizer. The tracer solution was mixed online with sample aerosol before reaching the plasma. Masses measured were: ^{201}Hg (flyback), ^{202}Hg, ^{203}Tl, ^{204}Pb, ^{205}Tl, ^{206}Pb, ^{207}Pb, ^{233}U, ^{235}U, ^{236}U, ^{238}U, ^{249}UO, ^{252}UO and ^{254}UO. Oxides have been reconverted to elemental intensities and added to the corresponding isotopes. No common-Pb correction was applied considering very low ^{204}Pb intensities and negligible effect on the final ages. Due to differing grain sizes, both rastering and spot mode were applied. Typically, rastering acquisition consisted of 1400 readings, comprising ~350 blank and solution readings and ~1050 data readings, whereas spot acquisition comprised ~200 blank and solution readings and ~500 data readings. Output laser energy varied between 120 and 160 mJ/pulse with a 30-μm beam diameter at a repetition rate of 10 Hz for rastering and 4 Hz for spot, respectively. Helium was used as a carrier gas (~1.1 L/min) of the ablated material from the ablation cell. Raw data were processed through the software LAMDATE, coded by J. Košler, which data correction by the intercept method (Sylvester and Ghaderi, 1997).

External correction of laser-induced Pb/U fractionation was monitored by repeated measurements of two reference zircons with known ages, Plešovice (337.13 ± 0.37 Ma) (Sláma et al., 2008) and 91500 (1065.4 ± 0.3 Ma; Wiedenbeck et al., 1995). The ages measured during this study for Plešovice zircon show a reasonable precision, accuracy and reproducibility (337.3 ± 2.8 Ma; 2σ; n = 66), consistent with recommended values. The 91500 zircon standard reproduced at 1076.0 ± 13.0 Ma (2σ; n = 11) which is in excellent agreement with recommended values.

3.2. $^{40}Ar/^{39}Ar$ geochronology

Unaltered, undeformed, inclusion-free hornblende and biotite were hand-picked and mineral concentrates were cleaned in an ultrasonic bath for 5 min in distilled water (biotite, plagioclase) and weak 5% $HNO_{3\ (aq)}$ (hornblende). Plagioclase concentrates were separated from quartz using centrifugal separation and sodium polytungstate. Samples were irradiated for either 30 h (Early Cretaceous and older samples) or 15 h (Late Cretaceous and younger samples) in the CLICIT facility of the TRIGA reactor at the Oregon State University. Fish Canyon Tuff sanidine was used as a flux monitor assuming a standard age of 28.02 ± 0.28 Ma (Renne et al., 1998), and J

Table 2
Major oxide and trace element, including REE data from selected rocks of the Western Cordillera, Cauca–Patía Valley and the Central Cordillera of Colombia.

Samples	DV74	DV106	DV111	DV26	DV58	DV138	DV156	DV91	DV79	DV126	DV165	DV43	DV175	DV178	DV29	DV87	DV90
Unit	Volcanic Fm. (Barroso Fm.)	Volcanic Fm.	Amaime Fm.	Córdoba Pluton	Antioquia Batholith	Saldaña Fm.	Sonsón Batholith	Buga Batholith	Dabeiba Fm.	Ricaurte arc	Mande Batholith	Quebradagrande complex	Quebradagrande complex	Quebradagrande complex	Arquía Complex	Arquía Complex	Arquía Complex
Lithology	Basalt	Gabbro	Basalt	Granodiorite	Granite	Rhyolite	Granite	Diorite	Basaltic andesite	Andesite	Diorite	Gabbro	Basaltic andesite	Basalt	Garnet amphibolite	Mica schist	Amphibolite
Latitude N	6°00′07.0″	3°46′04.0″	3°25′ 07.4″	4°24′30.9″	6°01′06.3″	1°06′ 45.0″	5°45′ 14.3″	3°55′ 31.0″	7°00′ 54.2″	1°13′ 17.5″	5°46′ 04.7″	6°05′36.8″	5°24′49.4″	5°37′05.7″	4°22′47.1″	4°18′ 15.1″	4°15′51.4″
Longitude W	75°47′34.2″	76°40′ 38.9″	76°11′ 10.7″	75°41′24.2″	75°08′ 10.8″	76°50′ 18.6″	75°18′ 00.5″	76°14′ 42.4″	76°18′ 16.0″	78°03′ 44.5″	76°14′ 56.3″	75°39′09.0″	75°28′30.3″	75°30′16.3″	75°43′09.0″	75°46′ 58.5″	75°47′23.9″
SiO2	49.15	49.80	49.59	60.30	70.08	63.68	68.34	50.99	50.00	56.92	60.69	50.45	51.05	51.63	47.33	47.02	48.15
TiO2	0.96	0.99	0.84	0.65	0.24	0.45	0.44	0.31	0.93	0.54	0.58	1.52	0.87	0.62	1.13	1.88	1.92
Al2O3	14.28	13.81	14.36	16.98	17.05	16.03	14.78	13.50	17.19	15.05	16.01	13.67	18.01	17.82	19.16	15.40	14.50
Fe2O3	10.85	9.40	10.55	5.55	1.69	3.66	3.76	9.38	9.43	7.11	6.93	11.56	7.67	7.96	8.33	12.20	12.16
MnO	0.34	0.16	0.18	0.09	0.03	0.09	0.07	0.17	0.30	0.22	0.16	0.21	0.12	0.16	0.28	0.18	0.20
MgO	8.39	9.45	9.04	1.68	0.69	1.21	1.94	10.84	2.73	4.22	2.79	7.30	6.00	3.30	5.86	6.76	7.87
CaO	9.36	9.96	12.73	5.61	3.31	2.94	3.62	11.31	9.12	9.24	6.12	9.70	5.45	9.97	12.02	12.35	10.37
Na2O	3.01	3.56	1.55	5.00	3.38	4.26	3.35	1.31	2.57	4.65	3.17	3.37	3.28	2.04	1.36	2.56	3.28
K2O	0.05	0.11	0.08	0.68	1.14	3.96	3.03	0.17	2.67	0.35	2.00	0.09	2.70	1.12	0.33	0.17	0.15
P2O5	0.08	0.07	0.07	0.19	0.06	0.12	0.10	0.04	0.48	0.09	0.14	0.13	0.21	0.39	0.04	0.18	0.17
LOI	3.51	3.07	1.39	2.68	1.95	2.83	0.46	2.30	4.02	0.98	0.59	2.40	3.64	4.03	4.06	1.81	1.26
Cr2O3	0.05	0.03	0.07	0.00	0.00	0.00	0.01	0.09	0.00	0.01	0.00	0.02	0.06	0.01	0.05	0.04	0.05
NiO	0.02	0.01	0.02	0.00	0.00	0.00	0.00	0.02	0.00	0.00	0.00	0.01	0.01	0.00	0.02	0.01	0.01
Total	100.03	100.41	100.47	99.42	99.61	99.24	99.91	100.42	99.43	99.38	99.18	100.43	99.07	99.07	99.96	100.54	100.07
Cr	324	180	443	10	18	9	43	618	7	71	12	128	394	61	357	279	334
Ni	134	131	147	6	4	5	11	164	4	22	5	67	112	22	159	102	99
Cu	n.d.	n.d.	n.d.	n.d.	2.00	18.00	4.00	n.d.	n.d.	17	72	n.d.	37	118	n.d.	n.d.	n.d.
Zn	81	59	76	45	41	56	58	69	98	60	57	103	89	90	156	99	60
Ga	37.01	17.93	13.84	78.81	16.25	15.60	15.65	19.75	97.95	11.60	13.60	13.99	23.80	17.37	64.25	11.41	17.70
Sc	52.47	51.48	49.29	8.07	4.49	8.67	11.70	51.84	27.70	30.50	19.08	43.83	25.43	19.62	34.63	41.10	46.36
V	323	301	296	112	29	76	90	197	268	275	172	343	196	210	315	281	325
Co	42	40	45	10	3	7	8	47	25	21	15	38	30	19	44	37	38
Cs	0.25	0.10	0.05	2.11	2.20	3.44	5.69	1.66	0.60	0.07	0.61	0.23	0.50	1.47	1.02	0.07	0.14
Ba	162	39	16	414	175	1436	744	65	528	195	433	8	1243	296	300	3	34
Rb	1.15	1.78	1.20	19.60	43.38	97.07	109.77	3.97	59.79	4.84	37.36	1.27	35.38	21.85	6.26	0.55	1.33
Th	0.19	0.13	0.22	3.18	9.30	6.58	13.96	0.41	1.53	0.76	5.60	0.10	2.50	3.60	1.25	0.05	0.29
Nb	2.87	2.25	3.54	2.28	4.43	5.56	6.04	0.63	5.92	0.63	2.14	1.74	10.36	2.57	4.57	1.55	3.45
Ta	0.16	0.16	0.20	0.18	0.40	0.30	0.58	0.07	0.36	0.03	0.14	0.16	0.50	0.16	0.28	0.07	0.42
Sr	92	75	83	402	215	526	268	149	809	222	403	99	1012	1868	269	138	94
Zr	42	35	39	308	102	176	133	25	86	39	169	88	137	70	96	33	40
Hf	1.08	0.98	1.04	6.61	2.96	4.57	3.79	0.78	1.93	1.20	4.57	2.51	3.35	1.99	2.77	1.17	1.00
Y	17.61	15.45	15.51	12.84	12.66	18.55	19.49	7.09	22.52	13.72	27.61	33.61	16.92	16.79	24.59	22.09	17.21
Pb	3.31	0.43	9.07	2.69	15.42	10.36	10.62	0.60	3.01	2.07	2.66	1.16	2.73	8.25	12.35	0.33	0.47
U	0.08	0.06	0.07	1.37	1.83	1.93	4.22	0.11	0.77	0.29	1.62	0.04	1.18	1.33	1.04	0.05	0.28
La	2.28	1.85	2.82	15.42	19.25	25.38	28.71	1.70	12.02	5.63	19.41	2.93	16.29	13.82	6.09	1.09	2.81
Ce	6.67	5.29	6.96	29.17	33.72	47.93	54.81	4.09	26.13	13.10	39.43	10.04	36.45	29.99	13.70	5.40	6.82
Pr	0.97	0.86	0.94	3.24	3.28	5.09	5.93	0.58	3.51	1.93	5.31	1.55	4.73	3.86	1.87	1.12	1.21
Nd	5.18	4.20	4.87	14.41	10.86	18.24	21.59	3.04	14.09	8.81	22.36	9.34	20.24	17.02	9.05	6.79	5.12
Sm	1.51	1.85	1.56	2.20	1.86	3.42	4.09	0.62	3.64	2.02	4.96	3.33	4.51	3.77	2.49	2.62	1.52
Eu	0.62	0.73	0.64	1.10	1.23	0.90	0.70	0.38	1.24	0.73	1.14	0.90	1.51	1.09	0.97	0.98	0.61
Gd	2.24	2.36	1.95	2.27	1.81	3.01	3.63	1.06	4.30	2.31	4.72	4.85	3.99	3.15	3.02	3.50	3.20
Tb	0.38	0.46	0.40	0.31	0.29	0.46	0.55	0.21	0.62	0.34	0.75	0.87	0.54	0.50	0.55	0.65	0.40
Dy	3.26	2.85	2.69	2.07	1.87	2.83	3.06	1.22	4.11	2.16	4.26	6.03	2.86	2.73	4.57	4.26	3.42
Ho	0.67	0.62	0.55	0.49	0.39	0.58	0.63	0.28	0.77	0.52	0.95	1.23	0.58	0.60	0.89	0.82	0.78
Er	1.91	1.91	1.88	1.49	1.27	1.89	1.83	0.88	2.47	1.31	2.75	3.59	1.60	1.66	2.40	2.56	2.09
Tm	0.29	0.26	0.26	0.23	0.19	0.30	0.32	0.16	0.33	0.18	0.41	0.54	0.22	0.25	0.41	0.29	0.32
Yb	1.98	1.65	2.27	1.26	1.43	1.92	1.80	1.05	2.30	1.20	2.97	3.57	1.43	1.74	3.00	2.28	2.62
Lu	0.29	0.30	0.30	0.26	0.21	0.31	0.29	0.15	0.33	0.20	0.44	0.53	0.22	0.26	0.37	0.32	0.32

values were obtained via interpolation. Samples were analyzed via incremental heating using a 30W CO_2-IR laser, and a stainless-steel extraction line coupled with a multi-collector Argus mass spectrometer (GV Instruments), housed at the University of Geneva and equipped with four high-gain (10^{12} Ω resistivity) Faraday cups for the measurement of ^{36}Ar, ^{37}Ar, ^{38}Ar, and ^{39}Ar, and a single 10^{11} Ω-resistivity Faraday cup for ^{40}Ar measurements. Analytical details are presented in Marschik et al. (2008) and in the caption of Table 3.

3.3. Whole rock geochemistry

The least altered whole rock samples were crushed using a steel jaw crusher and powdered using an agate disc mill. Major and some trace elements were analyzed using a Philips PW 2400 XRF spectrometer at the University of Lausanne using the Rhodes traces methodology (e.g. Schütte, 2009). Uncertainties estimated from repeated measurement of standards are <2% (2σ) for major elements and <5% (2σ) for trace elements. Selected trace elements and rare earth element abundances were determined using a 193 nm Excimer laser coupled to a Perkin Elmer ELAN 6100 DRC quadrupole ICP–MS, by ablating glass bead fragments (recovered from previous XRF analyses) at the University of Lausanne. Ninety-second background measurements were followed by 30–40 s of raw data collection, and measurements were performed in triplicate for each sample. Two-σ uncertainties were <8% for REE and selected trace elements. Internal standardization was based on CaO (previously determined by XRF) by reference to the NIST SRM610 and SRM612 glass bead standards. Data reduction, including interference correction, was performed using the Matlab-based SILLS program (Guillong et al., 2008).

4. Results: U–Pb LA–ICP–MS

SEM–CL images and summary LA–ICP–MS U–Pb zircon age data ($^{206}Pb/^{238}U$) from specific regions of single grains are shown in Figs. 3 and 4. Detailed LA–ICP–MS results are shown in Villagómez (2010) and all errors are reported at the 2σ-level.

4.1. Autochthonous rocks

4.1.1. Pre-Jurassic metamorphic and igneous rocks of the Tahami Terrane

Zircons extracted from a Paleozoic orthogneiss exposed in northern Colombia (La Miel orthogneiss; DV50; Fig. 2A) host complex inherited crystals with xenocrystic cores that yield ages spanning from 1700 to 900 Ma (Fig. 3), with a major peak at 1200 Ma. Two analyses of the oscillatory rim yielded ages of 470–440 Ma, which we interpret as the time of crystallization of the protolith.

A granitoid body located at the eastern border of the Central Cordillera in central Colombia (DV82; Fig. 2B) shows a bimodal age distribution with a major peak yielding a weighted mean age of 271.9 ± 3.7 Ma (MSWD = 1.2) from euhedral zircons, and a minor peak at ~305 Ma obtained from xenocrystic cores (Fig. 3). Euhedral to subhedral zircons from a white mica-bearing, granodioritic gneiss that is mapped as part of the Cajamarca Complex (DV18; Fig. 2B) located to the east of the Palestina Fault in central Colombia yielded a weighted mean average of 236.2 ± 6.3 Ma (MSWD = 0.61). A quartzite of the Cajamarca Complex (DV19) found at the same locality as gneiss DV18 yielded several detrital U–Pb age populations with a major peak at ~240 Ma and less prominent populations at ~600–500 Ma and ~1200–1000 Ma (Fig. 3). Finally, zircons from a paragneiss of the Cajamarca Complex (DV02; Fig. 3), located in central Colombia, east of the Otú–Pericos Fault (Fig. 2B) show several detrital zircon age populations. The small number of analyses (n = 12) inhibits the extraction of useful age populations, although it is significant that the youngest ages range between 270 and 220 Ma.

4.1.2. Jurassic–Cretaceous intrusions into continental crust

A granite of the Ibagué Batholith (DV09; Fig. 2B) exposed within a brittle deformed zone related to the Ibagué Fault in central Colombia yielded a weighted mean zircon U–Pb age of 159.5 ± 2.4 (MSWD 0.63; Fig. 3), which we consider to approximate the emplacement age of the sample. A less precise emplacement $^{206}Pb/^{238}U$ age of 166.0 ± 10.0 Ma was obtained from granodiorite (DV05) of the Ibagué batholith, located within 10 km of granite DV09. The youngest zircon age was derived from discordant isotopic data, and was excluded from the calculation of the weighted mean.

Granite DV56 forms part of the large Antioquia Batholith located in the northern Central Cordillera (Fig. 2A) and yields a weighted mean $^{206}Pb/^{238}U$ age of 87.2 ± 1.6 Ma (MSWD 0.81; Fig. 3). Granite DV58 also forms part of the Antioquia Batholith (Fig. 2A) and yields an older weighted mean age of 93.5 ± 1.5 Ma and a MSWD of 1.3.

Euhedral, zoned zircons from the small Córdoba pluton (granodiorite DV26; Fig. 2B), which intrudes the Quebradagrande Complex along the western flank of the Central Cordillera in central Colombia, yielded a weighted mean age of 79.7 ± 2.5 Ma (Fig. 3, MSWD 0.27), which is considered to represent the time of emplacement.

4.2. Quebradagrande unit

Euhedral zircon crystals from a metatuff of the Quebradagrande Complex taken close to the San Jerónimo Fault, yield a zircon U–Pb age of 114.3 ± 3.8 Ma (DV20; MSWD = 2.0; Fig. 4), which overlaps with Hautevarian — early Albian fossil ages for this unit (González, 1980).

4.3. Late Cretaceous allochthonous rocks exposed in the Cauca–Patía Valley and the Western Cordillera

A hornblende gabbro (Palmar gabbro; DV42) that is mapped as part of the Volcanic Fm. (Fig. 2B) yielded a weighted mean $^{206}Pb/^{238}U$ age of 99.7 ± 1.3 Ma (Fig. 4; MSWD 0.62). Large (>400 μm) euhedral zircon crystals extracted from two hornblende and biotite-bearing pegmatites exposed in the Bolívar Ultramafic Complex (Fig. 2B) yielded indistinguishable weighted mean $^{206}Pb/^{238}U$ ages of 95.5 ± 1.1 Ma (DV94; MSWD = 0.26) and 97.1 ± 2.0 Ma (DV95; MSWD = 1.2; Fig. 4). Both the Palmar gabbro and the Bolívar Ultramafic Complex form part of the magmatic basement of the Calima Terrane (Nivia, 2001), which is exposed in the Western Cordillera and is widely considered to represent a detached sliver of the Caribbean Large Igneous Province (Kerr et al., 2004).

A medium-grained lithic tuff (DV108), which is intercalated in hemipelagic turbidites of the marine Espinal Fm., located within the central Western Cordillera (Fig. 2B), yielded zoned euhedral zircons with a weighted mean age of 75.5 ± 1.6 Ma (Fig. 4; MSWD = 0.56), which represents a maximum depositional age for the Espinal Fm. This age corroborates the presence of Upper Cretaceous radiolarites (Aspden, 1984; Barrero, 1979; Etayo-Serna, 1985a) within the Espinal Fm., which lies unconformably on top of the Volcanic Fm. (Moreno-Sanchez and Pardo-Trujillo, 2002, 2003).

Magmatic zircon crystals from a granodiorite (DV30) of the Buga Batholith, which intrudes the Amaime Fm. and crops out within the Cauca–Patía Valley, west of the Romeral Fault System (Fig. 2B) yielded

Notes to Table 2
Oxide concentrations are presented as wt.% and were determined using XRF.
Trace element abundances are reported as ppm and were obtained using the ICP–MS method.
All analyses performed at the University of Lausanne.

Table 5
Major oxide and trace element, including REE data from the Western Cordillera, Cauca–Patía Valley and the Central Cordillera of Colombia.

Samples	DV38	DV39	DV40	DV74	DV75	DV102	DV103	DV104	DV105	DV106	DV109
Unit	Volcanic Fm.	Volcanic Fm.	Volcanic Fm.	Volcanic Fm. (Barroso Fm.)	Volcanic Fm. (Barroso Fm.)	Volcanic Fm. (Zabaletas Stock)	Volcanic Fm.	Volcanic Fm.	Volcanic Fm.	Volcanic Fm.	Volcanic Fm.
Lithology	Diabase	Gabbro	Dolerite	Basalt	Basalt	Gabbro-diorite	Basalt	Basalt	Basalt	Gabbro	Basalt
Latitude N	3°46′23.6″	3°27′48.3″	3°28′40.9″	6°00′07.0″	5°53′43.4″	3°49′10.6″	3°48′57.5″	3°46′46.6″	3°46′31.0″	3°46′04.0″	3°47′43.6″
Longitude W	76°44′23.9″	76°35′13.5″	76°38′47.7″	75°47′34.2″	75°54′05.8″	76°36′00.7″	76°36′31.8″	76°43′24.3″	76°41′55.3″	76°40′38.9″	76°38′01.4″
SiO_2	47.07	49.89	50.16	49.15	50.12	62.90	49.68	46.86	43.60	49.80	49.32
TiO_2	1.27	1.47	1.08	0.96	0.97	1.76	1.03	1.03	2.51	0.99	1.20
Al_2O_3	15.28	12.99	13.82	14.28	13.81	13.05	13.66	15.01	12.73	13.81	14.15
Fe_2O_3	11.48	13.91	11.87	10.85	10.27	3.19	11.42	11.43	18.92	9.40	12.64
MnO	0.20	0.20	0.19	0.34	0.18	0.04	0.17	0.18	0.24	0.16	0.20
MgO	7.37	5.78	7.55	8.39	7.70	5.14	8.16	8.31	6.56	9.45	7.61
CaO	11.18	10.25	11.53	9.36	13.27	6.03	10.39	12.80	8.27	9.96	10.37
Na_2O	2.53	2.17	2.14	3.01	1.88	5.64	2.86	1.89	2.99	3.56	2.56
K_2O	0.95	0.04	0.13	0.05	0.07	0.09	0.12	0.22	0.06	0.11	0.13
P_2O_5	0.09	0.13	0.08	0.08	0.08	0.17	0.08	0.09	0.23	0.07	0.10
LOI	2.25	3.34	1.34	3.51	2.01	1.61	2.94	2.62	2.94	3.07	2.16
Cr_2O_3	0.04	0.01	0.03	0.05	0.07	0.00	0.04	0.06	0.01	0.03	0.04
NiO	0.01	0.01	0.01	0.02	0.02	0.00	0.01	0.02	0.01	0.01	0.02
Total	99.71	100.18	99.92	100.03	100.44	99.60	100.56	100.51	99.07	100.41	100.50
Cr	261	51	203	324	430	3	208	394	39	180	245
Ni	106	57	110	134	137	21	130	149	42	131	136
Cu	n.d.	n.d.	n.d.	n.d.	n.d.	n.d.	n.d.	n.d.	n.d.	n.d.	n.d.
Zn	92	107	90	81	75	14	83	89	190	59	101
Ga	85.15	17.86	18.06	37.01	15.21	16.20	21.24	68.09	31.93	17.93	18.36
Sc	50.21	47.87	55.42	52.47	46.04	41.84	51.55	48.83	43.34	51.48	52.04
V	344	426	360	323	299	450	345	312	540	301	392
Co	44	44	46	42	39	8	43	48	50	40	45
Cs	0.28	0.09	0.17	0.25	0.06	0.04	0.03	0.12	0.78	0.10	0.10
Ba	467	15	34	162	21	14	60	316	93	39	25
Rb	10.48	1.05	1.45	1.15	1.34	1.52	1.45	2.46	1.33	1.78	1.64
Th	0.26	0.38	0.24	0.19	0.38	0.50	0.20	0.16	0.79	0.13	0.20
Nb	2.94	5.29	3.39	2.87	5.23	7.29	3.32	2.65	10.69	2.25	3.75
Ta	0.32	0.40	0.39	0.16	0.34	0.50	0.23	0.21	0.73	0.16	0.25
Sr	131	59	112	92	104	26	145	214	43	75	97
Zr	64	72	48	42	46	133	45	45	148	35	52
Hf	1.56	2.05	1.29	1.08	1.34	3.78	1.21	1.39	4.36	0.98	1.27
Y	23.15	29.06	18.73	17.61	15.63	42.65	18.38	18.59	50.40	15.45	21.97
Pb	1.20	0.70	0.62	3.31	0.52	1.24	0.37	0.54	0.96	0.43	0.54
U	0.12	0.13	0.34	0.08	0.07	0.07	0.09	0.08	0.21	0.06	0.10
La	2.89	4.26	2.90	2.28	3.87	3.82	2.60	2.42	8.26	1.85	3.14
Ce	8.30	10.78	8.67	6.67	9.66	11.03	6.89	6.88	22.14	5.29	8.29
Pr	1.33	1.82	1.28	0.97	1.47	1.78	0.97	1.07	3.34	0.86	1.20
Nd	7.84	7.99	7.27	5.18	7.11	10.48	5.97	6.56	18.21	4.20	6.15
Sm	1.96	3.06	2.51	1.51	1.82	3.62	2.20	2.30	5.59	1.85	2.21
Eu	0.97	1.02	0.73	0.62	0.64	1.01	0.62	0.78	1.67	0.73	0.89
Gd	3.08	3.30	2.55	2.24	1.89	5.08	2.34	2.85	7.27	2.36	3.45
Tb	0.64	0.86	0.55	0.38	0.43	0.91	0.52	0.51	1.36	0.46	0.60
Dy	4.10	5.58	3.67	3.26	2.85	6.85	3.47	3.50	9.36	2.85	4.18
Ho	0.85	1.25	0.65	0.67	0.61	1.60	0.72	0.71	1.87	0.62	0.80
Er	2.55	3.36	2.44	1.91	1.74	4.56	2.04	2.03	5.67	1.91	2.41
Tm	0.43	0.51	0.61	0.29	0.22	0.77	0.32	0.28	0.89	0.26	0.35
Yb	2.38	3.90	2.04	1.98	1.93	4.92	2.10	1.85	6.01	1.65	2.88
Lu	0.42	0.51	0.27	0.29	0.30	0.70	0.31	0.32	0.83	0.30	0.39

Oxide concentrations are presented as wt.% and were determined using XRF.
Trace element abundances are reported as ppm and were obtained using the ICP–MS method.
All analyses performed at the University of Lausanne.

a weighted mean U–Pb age of 92.1 ± 0.8 Ma (MSWD = 0.66; Fig. 4). Similarly, a diorite (DV91) of the same intrusion yielded a less precise but indistinguishable age of 90.6 ± 1.3 Ma (MSWD = 0.38; Fig. 4).

5. Results: $^{40}Ar/^{39}Ar$

Age spectra and inverse isochrons acquired from hornblende, biotite and plagioclase are shown in Fig. 5 and all errors are reported at the 2σ-level.

5.1. Autochthonous rocks of the Tahami Terrane

A majority of hornblendes extracted from diorites and granites of the Jurassic Ibagué Batholith in the Central Cordillera yielded plateau ages (Fig. 5) according to the definition of Lanphere and Dalrymple (1978), which are indistinguishable from their inverse isochron ages. Hornblende from granite DV04 yielded a plateau age of 159.2 ± 5.2 Ma (80% of ^{39}Ar released) with no evidence of excess ^{40}Ar. Similar Late Jurassic ages were obtained from granitoids DV05 (U–Pb zircon age 166.0 ± 10.0 Ma; Section 4.1.2) and DV07, which yielded mean weighted plateau ages of

DV110	DV111	DV112	DV26	DV58	DV138	DV156	DV30	DV91	DV78	DV79	DV122	DV125
Amaime Fm.	Amaime Fm.	Amaime Fm.	Córdoba Pluton	Antioquia Batholith	Saldaña Fm.	Sonsón Batholith	Buga Batholith	Buga Batholith	Dabeiba Fm.	Dabeiba Fm.	Ricaurte arc	Ricaurte arc
Basalt	Basalt	Basalt	Granodiorite	Granite	Rhyolite	Granite	Granodiorite	Diorite	Andesite	Basaltic andesite	Porphyritic basalt	Andesite
3°33′20.0″	3°25′07.4″	3°18′36.2″	4°24′30.9″	6°01′06.3″	1°06′45.0″	5°45′14.3″	3°54′10.6″	3°55′31.0″	7°00′54.9″	7°00′54.2″	1°12′08.1″	1°16′33.6″
76°11′10.0″	76°11′10.7″	76°11′36.7″	75°41′24.2″	75°08′10.8″	76°50′18.6″	75°18′00.5″	76°10′50.4″	76°14′42.4″	76°18′29.5″	76°18′16.0″	77°58′42.2″	78°05′40.1″
49.27	49.59	49.36	60.30	70.08	63.68	68.34	67.60	50.99	52.09	50.00	49.85	49.52
0.84	0.84	0.96	0.65	0.24	0.45	0.44	0.28	0.31	0.62	0.93	0.65	0.69
14.23	14.36	14.13	16.98	17.05	16.03	14.78	14.47	13.50	17.08	17.19	18.27	15.65
11.12	10.55	10.22	5.55	1.69	3.66	3.76	5.24	9.38	7.87	9.43	9.86	8.97
0.19	0.18	0.16	0.09	0.03	0.09	0.07	0.09	0.17	0.18	0.30	0.11	0.14
8.25	9.04	8.95	1.68	0.69	1.21	1.94	2.58	10.84	2.38	2.73	4.87	8.67
11.29	12.73	11.95	5.61	3.31	2.94	3.62	5.57	11.31	5.85	9.12	8.63	9.83
2.62	1.55	2.41	5.00	3.38	4.26	3.35	3.38	1.31	4.73	2.57	3.00	1.86
0.45	0.08	0.19	0.68	1.14	3.96	3.03	0.72	0.17	3.94	2.67	1.10	0.62
0.07	0.07	0.09	0.19	0.06	0.12	0.10	0.07	0.04	0.43	0.48	0.17	0.11
1.91	1.39	1.80	2.68	1.95	2.83	0.46	0.45	2.30	4.59	4.02	2.87	3.47
0.06	0.07	0.07	0.00	0.00	0.00	0.01	0.01	0.09	0.00	0.00	0.01	0.04
0.02	0.02	0.02	0.00	0.00	0.00	0.00	0.00	0.02	0.00	0.00	0.00	0.01
100.33	100.47	100.30	99.42	99.61	99.24	99.91	100.46	100.42	99.76	99.43	99.37	99.58
377	443	456	10	18	9	43	53	618	8	7	49	240
147	147	176	6	4	5	11	19	164	4	4	23	93
n.d.	n.d.	n.d.	n.d.	2.00	18.00	4.00	n.d.	n.d.	n.d.	n.d.	112	41
75	76	72	45	41	56	58	41	69	83	98	87	71
15.06	13.84	17.49	78.81	16.25	15.60	15.65	41.53	19.75	101.80	97.95	16.49	13.26
50.64	49.29	52.29	8.07	4.49	8.67	11.70	18.90	51.84	17.78	27.70	30.03	35.30
348	296	312	112	29	76	90	127	197	217	268	381	253
42	45	45	10	3	7	8	12	47	17	25	27	33
0.09	0.05	0.08	2.11	2.20	3.44	5.69	0.38	1.66	0.92	0.60	0.38	0.55
20	16	24	414	175	1436	744	204	65	578	528	106	55
11.95	1.20	4.13	19.60	43.38	97.07	109.77	12.19	3.97	75.91	59.79	24.86	12.40
0.18	0.22	0.50	3.18	9.30	6.58	13.96	1.00	0.41	1.74	1.53	0.73	0.59
2.49	3.54	4.92	2.28	4.43	5.56	6.04	1.73	0.63	4.54	5.92	0.64	0.99
0.15	0.20	0.29	0.18	0.40	0.30	0.58	0.27	0.07	0.29	0.36	0.04	0.06
91	83	101	402	215	526	268	196	149	661	809	481	295
38	39	51	308	102	176	133	66	25	91	86	48	35
0.99	1.04	1.32	6.61	2.96	4.57	3.79	1.75	0.78	2.43	1.93	1.38	1.14
17.60	15.51	18.19	12.84	12.66	18.55	19.49	9.17	7.09	21.61	22.52	15.55	14.26
0.74	9.07	0.71	2.69	15.42	10.36	10.62	1.62	0.60	4.17	3.01	2.63	1.07
0.06	0.07	0.20	1.37	1.83	1.93	4.22	0.40	0.11	1.00	0.77	0.21	0.14
1.99	2.82	3.80	15.42	19.25	25.38	28.71	4.54	1.70	13.94	12.02	7.36	4.64
5.99	6.96	9.06	29.17	33.72	47.93	54.81	10.23	4.09	28.19	26.13	17.45	11.31
0.86	0.94	1.25	3.24	3.28	5.09	5.93	1.36	0.58	3.67	3.51	2.63	1.78
4.96	4.87	7.36	14.41	10.86	18.24	21.59	5.82	3.04	17.19	14.09	12.07	8.84
1.90	1.56	1.79	2.20	1.86	3.42	4.09	2.59	0.62	4.21	3.64	3.02	2.35
0.59	0.64	0.63	1.10	1.23	0.90	0.70	0.48	0.38	1.17	1.24	0.99	0.79
1.91	1.95	2.34	2.27	1.81	3.01	3.63	1.84	1.06	4.19	4.30	2.93	2.63
0.46	0.40	0.44	0.31	0.29	0.46	0.55	0.31	0.21	0.60	0.62	0.45	0.41
2.89	2.69	2.79	2.07	1.87	2.83	3.06	2.05	1.22	3.81	4.11	2.67	2.57
0.68	0.55	0.70	0.49	0.39	0.58	0.63	0.50	0.28	0.80	0.77	0.60	0.50
1.86	1.88	2.15	1.49	1.27	1.89	1.83	1.46	0.88	2.34	2.47	1.72	1.58
0.30	0.26	0.28	0.23	0.19	0.30	0.32	0.26	0.16	0.32	0.33	0.24	0.21
1.97	2.27	1.97	1.26	1.43	1.92	1.80	1.23	1.05	2.23	2.30	1.55	1.58
0.36	0.30	0.28	0.26	0.21	0.31	0.29	0.27	0.15	0.32	0.33	0.23	0.23

153.1 ± 2.0 Ma (85% of ^{39}Ar released) and 148.9 ± 3.4 Ma (50% of ^{39}Ar released), with initial ^{40}Ar/^{36}Ar ratios that overlap with the atmospheric value of 295.5 (Steiger and Jäger, 1977). Hornblende from granite DV06 yielded a disturbed, stair-case age spectrum with low temperature step-ages of ~140 Ma that increase to ~180 Ma in the three highest temperature steps that yielded <50% of the total ^{39}Ar released.. The hornblende was unaltered and free of inclusions, and we tentatively interpret the age spectrum to be a consequence of Ar loss during either slow cooling, or post-crystallization reheating at some point during the Cretaceous. The oldest age of ~180 Ma may approximate the timing of crystallization, although it is older than U–Pb zircon ages acquired from other samples of the Ibagué Batholith.

Biotite from granite DV07 of the Ibagué Batholith yielded a ^{40}Ar/^{39}Ar plateau age of 147.0 ± 0.5 Ma (Fig. 5), which is indistinguishable from its hornblende age of 148.9 ± 3.4 Ma, suggesting the sample cooled rapidly from >550 °C to <300 °C (closure temperature of hornblende and biotite, respectively; McDougall and Harrison, 1999) during 150–147 Ma, as a consequence of thermal relaxation subsequent to magmatic emplacement. Granite DV09 of the Ibagué Batholith yielded a weighted mean age of 151.8 ± 0.9 Ma over the

Table 5 (*continued*)

Samples	DV126	DV165	DV167	DV43	DV48	DV159	DV171	DV173	DV174
Unit	Ricaurte arc	Mande Bath	Mande Bath	Quebradagrande complex	Quebradagrande complex	Quebradagrande complex	Quebradagrande complex	Quebradagrande complex	Quebradagrande complex
Lithology	Andesite	Diorite	Granodiorite	Gabbro	Gabbro-diorite	Andesite	Andesite	Basalt	Basaltic andesite
Latitude N	1°13′17.5″	5°46′04.7″	5°46′15.1″	6°05′36.8″	6°07′07.7″	4°55′36.7″	5°20′51.0″	5°23′31.7″	5°24′49.4″
Longitude W	78°03′44.5″	76°14′56.3″	76°14′51.1″	75°39′09.0″	75°43′59.5″	75°37′25.7″	75°28′53.0″	75°28′26.8″	75°28′30.3″
SiO_2	56.92	60.69	60.05	50.45	46.19	60.40	58.87	48.20	57.58
TiO_2	0.54	0.58	0.56	1.52	1.46	0.77	0.70	1.63	0.74
Al_2O_3	15.05	16.01	16.25	13.67	15.23	17.16	17.79	14.19	17.06
Fe_2O_3	7.11	6.93	7.06	11.56	10.14	5.63	5.05	11.26	5.42
MnO	0.22	0.16	0.15	0.21	0.16	0.08	0.08	0.19	0.08
MgO	4.22	2.79	2.76	7.30	8.99	2.91	3.07	6.18	3.16
CaO	9.24	6.12	5.94	9.70	14.01	5.37	3.90	8.79	3.50
Na_2O	4.65	3.17	3.17	3.37	2.18	4.22	5.85	3.11	6.04
K_2O	0.35	2.00	2.35	0.09	0.04	1.85	1.08	0.92	0.99
P_2O_5	0.09	0.14	0.15	0.13	0.09	0.24	0.19	0.17	0.21
LOI	0.98	0.59	0.68	2.40	1.69	0.56	2.63	4.66	4.43
Cr_2O_3	0.01	0.00	0.00	0.02	0.07	0.01	0.01	0.03	0.01
NiO	0.00	0.00	0.00	0.01	0.01	0.00	0.00	0.01	0.00
Total	99.38	99.18	99.11	100.43	100.25	99.19	99.22	99.33	99.21
Cr	71	12	8	128	506	73	54	220	43
Ni	22	5	4	67	127	23	33	81	27
Cu	17	72	64	n.d.	n.d.	16	29	31	36
Zn	60	57	57	103	37	89	63	97	68
Ga	11.60	13.60	15.19	13.99	18.71	19.59	21.55	14.99	19.82
Sc	30.50	19.08	21.13	43.83	50.88	13.64	11.61	41.99	13.33
V	275	172	188	343	415	150	138	377	156
Co	21	15	16	38	43	13	15	40	14
Cs	0.07	0.61	0.81	0.23	0.13	1.85	0.38	0.50	0.27
Ba	195	433	587	8	12	1133	762	913	522
Rb	4.84	37.36	43.34	1.27	2.18	49.09	12.55	22.05	14.52
Th	0.76	5.60	3.89	0.10	0.19	5.26	2.54	0.15	2.63
Nb	0.63	2.14	2.37	1.74	3.09	4.81	9.71	2.23	10.53
Ta	0.03	0.14	0.10	0.16	0.20	0.29	0.59	0.15	0.56
Sr	222	403	416	99	282	597	656	241	466
Zr	39	169	147	88	135	120	127	98	138
Hf	1.20	4.57	4.15	2.51	3.67	3.19	3.27	2.70	3.36
Y	13.72	27.61	34.99	33.61	44.79	20.28	11.94	37.30	13.41
Pb	2.07	2.66	8.11	1.16	0.97	10.55	3.70	0.72	5.66
U	0.29	1.62	0.97	0.04	0.24	2.16	1.19	0.19	1.15
La	5.63	19.41	19.64	2.93	5.46	20.85	16.79	3.96	18.61
Ce	13.10	39.43	43.79	10.04	16.12	37.62	35.68	12.23	40.10
Pr	1.93	5.31	6.29	1.55	2.66	5.10	4.49	2.09	5.01
Nd	8.81	22.36	26.86	9.34	14.25	20.10	18.41	11.02	20.71
Sm	2.02	4.96	6.21	3.33	4.92	4.61	3.90	3.74	4.42
Eu	0.73	1.14	1.26	0.90	1.62	1.23	1.17	1.40	1.42
Gd	2.31	4.72	6.03	4.85	6.35	3.92	3.27	5.40	3.63
Tb	0.34	0.75	0.95	0.87	1.04	0.54	0.47	0.97	0.43
Dy	2.16	4.26	5.75	6.03	7.67	3.12	2.42	6.21	2.41
Ho	0.52	0.95	1.24	1.23	1.85	0.67	0.50	1.40	0.45
Er	1.31	2.75	3.52	3.59	4.96	1.86	1.21	4.10	1.25
Tm	0.18	0.41	0.52	0.54	0.85	0.27	0.22	0.60	0.21
Yb	1.20	2.97	3.32	3.57	4.77	1.77	1.25	3.72	1.35
Lu	0.20	0.44	0.55	0.53	0.73	0.28	0.22	0.57	0.21

flattest region of a disturbed age spectrum where individual step ages differ by less than 1% and account for ~70% of the total ^{39}Ar released. The same sample yielded a zircon U–Pb age of 159.5 ± 2.4 Ma, suggesting the biotite age may record slow cooling via thermal relaxation, subsequent to intrusion during the Late Jurassic.

A single $^{40}Ar/^{39}Ar$ hornblende age obtained from a gneiss of the Cajamarca Complex (DV02), located proximal (hundreds of meters) to the contact with the intruding Ibagué Batholith in central Colombia (Fig. 2B) yielded a plateau age of 155.6 ± 6.2 Ma (>50% of ^{39}Ar released; Fig. 5), which has a non-radiogenic $^{40}Ar/^{36}Ar$ intercept (MSWD 1.22) that is indistinguishable from atmospheric Ar. The $^{40}Ar/^{39}Ar$ hornblende age is significantly younger than the youngest U–Pb age (~220 Ma; Section 4.1.1) obtained from detrital zircons, and it is likely that it was reset by thermally activated diffusion during intrusion of the Ibagué Batholith.

A Permian granitoid body (DV82) located at the eastern border of the Central Cordillera in central Colombia (Fig. 2B), which gave a zircon U–Pb age of 271.9 ± 3.7 Ma (Section 4.1.1), yielded a disturbed $^{40}Ar/^{39}Ar$ age spectrum with a total fusion age of 225.3 ± 1.1 Ma (hornblende; Fig. 5) that is significantly younger than its emplacement age.

DV175	DV176	DV178	DV28	DV29	DV87	DV88	DV90	DV157	DV158
Quebradagrande complex	Quebradagrande complex	Quebradagrande complex	Arquía Complex	Arquía Complex	Arquía Complex	Arquía Complex	Arquía Complex	Arquía Complex	Arquía Complex
Basaltic andesite	Diorite	Basalt	Garnet white mica amphibolite	Garnet amphibolite	Mica schist	Amphibolitic schist	Amphibolite	Garnet amphibolite	Amphibolitic schist
5°24′49.4″	5°27′16.0″	5°37′05.7″	4°22′47.1″	4°22′47.1″	4°18′15.1″	4°18′02.9″	4°15′51.4″	4°17′13.1″	4°17′50.4″
75°28′30.3″	75°28′28.2″	75°30′16.3″	75°43′09.0″	75°43′09.0″	75°46′58.5″	75°46′41.1″	75°47′23.9″	75°47′05.7″	75°46′46.5″
51.05	64.91	51.63	48.71	47.33	47.02	49.30	48.15	51.46	46.90
0.87	0.42	0.62	2.18	1.13	1.88	1.65	1.92	2.23	2.25
18.01	17.22	17.82	14.37	19.16	15.40	14.57	14.50	13.06	13.43
7.67	2.97	7.96	11.97	8.33	12.20	11.13	12.16	12.90	13.69
0.12	0.06	0.16	0.20	0.28	0.18	0.18	0.20	0.20	0.21
6.00	2.39	3.30	8.07	5.86	6.76	7.42	7.87	6.01	7.56
5.45	2.13	9.97	9.69	12.02	12.35	10.27	10.37	8.38	9.87
3.28	6.27	2.04	2.32	1.36	2.56	3.24	3.28	4.04	3.33
2.70	0.94	1.12	0.35	0.33	0.17	0.06	0.15	0.16	0.11
0.21	0.17	0.39	0.22	0.04	0.18	0.15	0.17	0.19	0.21
3.64	2.02	4.03	1.52	4.06	1.81	1.73	1.26	0.53	1.50
0.06	0.01	0.01	0.03	0.05	0.04	0.04	0.05	0.03	0.04
0.01	0.00	0.00	0.01	0.02	0.01	0.01	0.01	0.01	0.02
99.07	99.50	99.07	99.63	99.96	100.54	99.75	100.07	99.19	99.11
394	51	61	204	357	279	293	334	176	300
112	34	22	73	159	102	94	99	49	141
37	2	118	n.d.	n.d.	n.d.	n.d.	n.d.	19	4
89	40	90	203	156	99	90	60	120	122
23.80	16.87	17.37	24.42	64.25	11.41	15.92	17.70	17.58	19.24
25.43	7.65	19.62	49.15	34.63	41.10	44.90	46.36	37.73	38.68
196	73	210	425	315	281	359	325	434	430
30	9	19	37	44	37	38	38	35	45
0.50	0.22	1.47	0.46	1.02	0.07	0.06	0.14	0.08	0.12
1243	243	296	61	300	3	9	34	12	16
35.38	15.94	21.85	4.72	6.26	0.55	0.46	1.33	0.92	1.54
2.50	3.83	3.60	0.18	1.25	0.05	0.35	0.29	0.26	0.18
10.36	17.14	2.57	3.13	4.57	1.55	2.87	3.45	2.51	2.62
0.50	0.98	0.16	0.21	0.28	0.07	0.20	0.42	0.16	0.14
1012	518	1868	141	269	138	119	94	69	130
137	110	70	135	96	33	99	40	137	137
3.35	2.88	1.99	3.59	2.77	1.17	2.60	1.00	3.68	3.60
16.92	7.76	16.79	46.21	24.59	22.09	35.26	17.21	48.47	49.71
2.73	2.88	8.25	6.64	12.35	0.33	0.58	0.47	2.01	0.58
1.18	1.38	1.33	1.31	1.04	0.05	0.11	0.28	0.10	0.10
16.29	20.03	13.82	4.97	6.09	1.09	4.22	2.81	5.00	5.20
36.45	36.09	29.99	15.57	13.70	5.40	12.91	6.82	16.73	17.48
4.73	3.77	3.86	2.67	1.87	1.12	2.07	1.21	2.79	2.88
20.24	13.35	17.02	15.27	9.05	6.79	11.73	5.12	15.40	15.98
4.51	2.20	3.77	4.67	2.49	2.62	3.97	1.52	5.32	5.37
1.51	0.67	1.09	2.01	0.97	0.98	1.29	0.61	1.66	1.68
3.99	1.98	3.15	7.03	3.02	3.50	4.98	3.20	7.20	7.23
0.54	0.23	0.50	1.25	0.55	0.65	0.92	0.40	1.32	1.34
2.86	1.33	2.73	8.44	4.57	4.26	6.19	3.42	8.34	8.30
0.58	0.30	0.60	1.91	0.89	0.82	1.22	0.78	1.79	1.84
1.60	0.77	1.66	5.44	2.40	2.56	3.95	2.09	5.14	5.42
0.22	0.12	0.25	0.68	0.41	0.29	0.54	0.32	0.74	0.75
1.43	0.74	1.74	4.93	3.00	2.28	3.60	2.62	5.08	5.20
0.22	0.12	0.26	0.71	0.37	0.32	0.55	0.32	0.72	0.76

5.2. Allochthonous rocks of the Western Cordillera and the Cauca–Patía Valley

Plagioclase separated from groundmass of andesite (DV78) of the Eocene (Kerr et al., 1997) Dabeiba Fm., which forms part of the Dabeiba Volcanic Arc located along the eastern flank of the northern Western Cordillera, yielded a total fusion age of 25.6 ± 2.6 Ma (Fig. 5) from a disturbed age spectrum. The Dabeiba Fm. forms part of the Chocó–Panamá Terrane, which is also considered to be underlain by oceanic plateau material (Kerr et al., 1997). Our age is distinguishably younger than a plagioclase $^{40}Ar/^{39}Ar$ age of 43.1 ± 0.4 Ma obtained by Kerr et al. (1997) from the same rocks.

6. Results: whole rock geochemistry

6.1. Jurassic to Cretaceous magmatism within the Tahami Terrane

Major oxide and trace element data (Table 2) have been acquired from i) a rhyolite of the Jurassic Saldaña Fm. (DV138), which is considered to be the extrusive component of continental arc rocks of

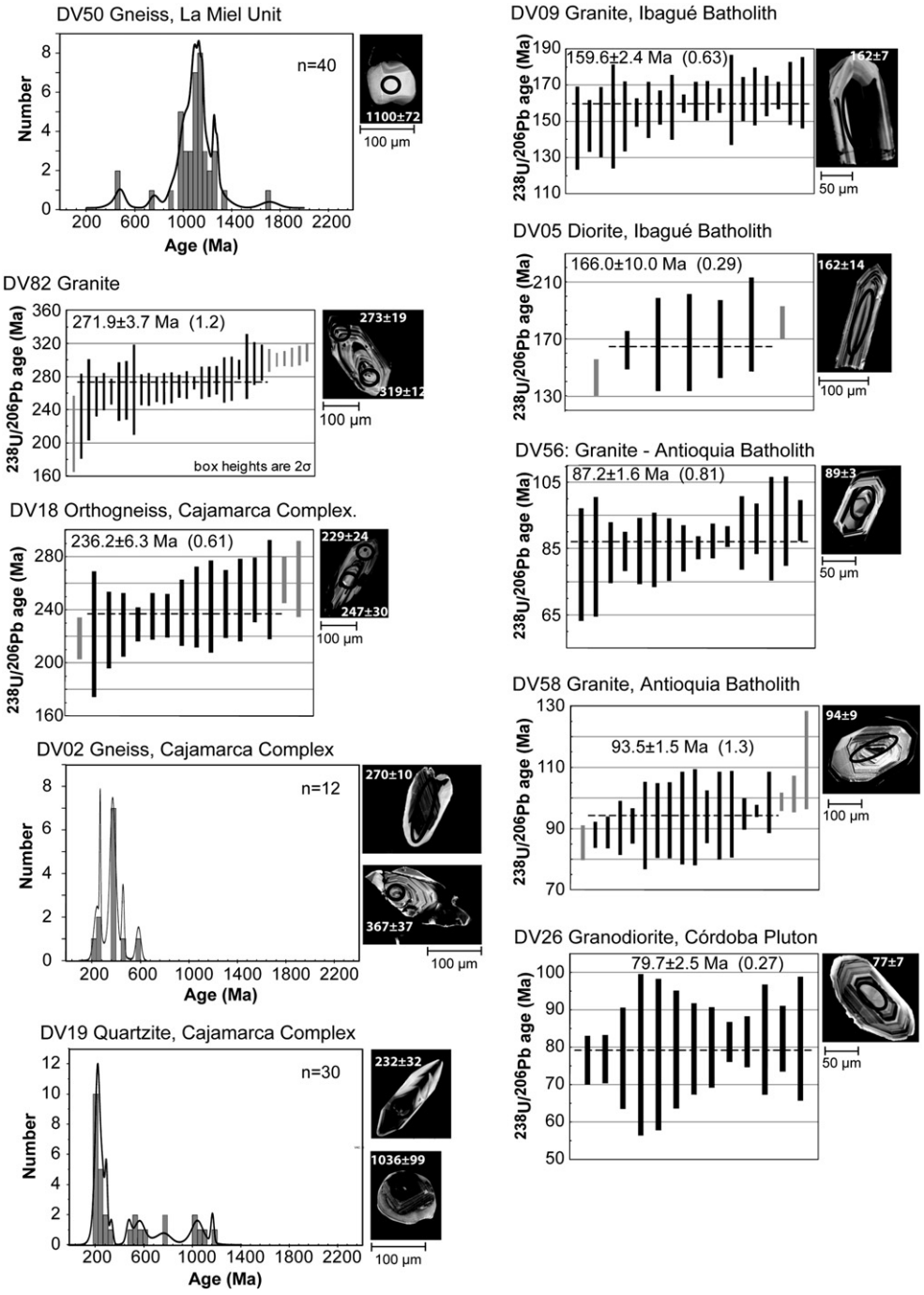

Fig. 3. $^{206}Pb/^{238}U$ ages acquired from zircons extracted from the Tahami Terrane using the LA–ICP–MS method, showing cathodoluminescence images of representative zircon grains; ablated regions are highlighted. Weighted mean ages are shown in bold and their associated MSWD in parentheses. Gray bars indicate analyses that were excluded from the weighted mean calculation due to the presence of suspect, xenocrystic and antecrystic components (after analyses of the CL images) or Pb loss, following the approach of Schütte (2009). Error bars and weighted mean uncertainties correspond to analytical error at the 2σ level. Histograms are shown with 40 Ma bins. All diagrams generated using the Isoplot v.3.31 Excel macro (Ludwig, 2003).

the Ibagué Batholith (Toussaint, 1995), ii) intrusive rocks of the Late Cretaceous Antioquia Batholith (DV58 and DV56; zircon U–Pb age spans 94–87 Ma), iii) the Late Cretaceous Córdoba Batholith (DV26; zircon U–Pb age of 79.7 ± 2.5 Ma), and iv) the Paleocene Sonsón Batholith (zircon U–Pb ages span 65–55 Ma; Ordóñez-Carmona et al., 2001). All of the sampled rocks are classified as granites and granodiorites on the Th–Co discrimination diagram (Fig. 6; Hastie et al., 2007) with SiO_2 values ranging between 60 and 70%, and fall into the calc-alkaline field within La/Yb v Zr/Th space (Fig. 6), corroborating LREE enrichment ($(La/Yb)_N$ 8.81 to 11.46). Multi-element plots (Fig. 7) reveal negative Nb–Ta and Ti anomalies and are indicative of a subduction-related origin.

6.2. Para-autochthonous rocks entrained within the Romeral Fault Zone

6.2.1. Igneous rocks of the Quebradagrande Complex

Basalts and gabbros (DV43, DV48 and DV173; SiO_2wt.% 46 to 50; MgO wt.% 6 to 9) of the Quebradagrande Complex (Fig. 2A–B) located along the western flank of the Central Cordillera are characterized by flat- to positive slopes on chondrite-normalized REE plots (La/Yb 0.8–

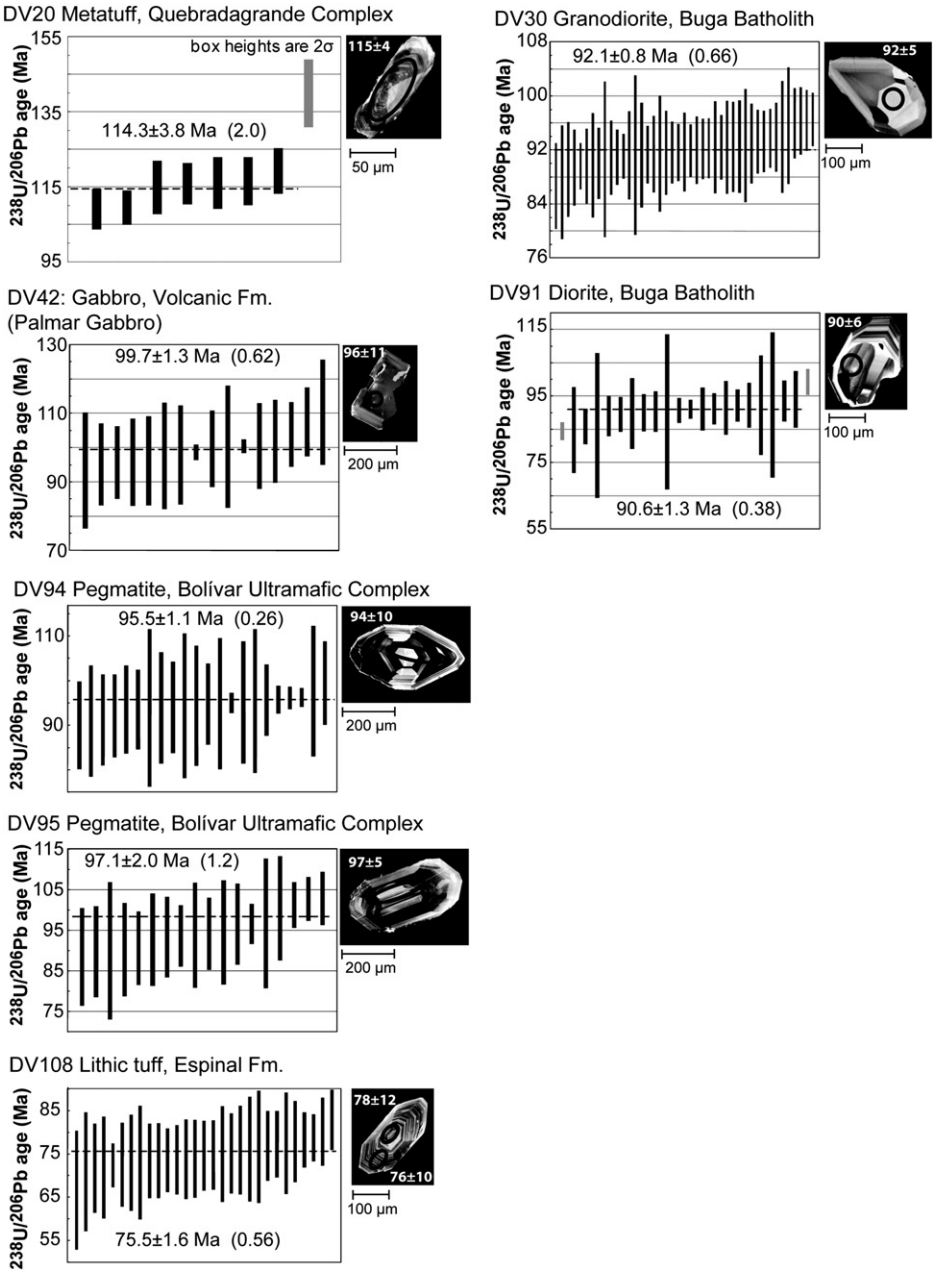

Fig. 4. $^{206}Pb/^{238}U$ ages acquired from zircons extracted from Quebradagrande Complex and accreted rocks of the Calima Terrane using the LA–ICP–MS method. Additional details are presented in Fig. 3.

1.1; Fig. 8), high Zr/Th ratios (>650) and low Th/Co ratios (<0.004; Fig. 6) that are indicative of a depleted mantle source origin such as at a mid-oceanic ridge, or perhaps enriched MORB material that may be indicative of the presence of volcanic seamounts. Negative Nb–Ta and Ti anomalies are not present suggesting that these rocks are not petrogenetically related to subduction zone magmatism.

All basaltic andesites and andesites (DV159, DV171, DV174, DV175, DV178; SiO2 wt.% 51 to 60; MgO wt.% 2 to 6), and a diorite (DV176; SiO2 wt.% 64; MgO wt.% 2) are less altered and metamorphosed than the basalts and gabbros. These magmatic rocks differ distinctly from the previous group because they yield negative Nb–Ta and Ti anomalies on a primitive-mantle normalized multi-element plot (Fig. 8), high La/Yb ratios of 7.9–26.9, low Zr/Th values (<55; Fig. 6) and Th abundances of >1 ppm, suggesting they are petrogenetically related to subduction and have a calc-alkaline signature. These rocks are strongly depleted in Y (<20 ppm) and HREE, and are enriched in Sr (>400 ppm). Uniformly elevated Sr contents and the absence of negative Eu anomalies (Fig. 8) suggest that the parental melts evolved at high pressures, outside the stability field of plagioclase but under the presence of garnet.

6.2.2. Arquía Complex

Garnet-bearing amphibolites of the Arquía Complex located along the western flank of the Central Cordillera (Fig. 2) display significant scatter in LILE (Fig. 8), which is indicative of remobilization via metamorphism and alteration processes. The amphibolites yield $(La/Sm)_N$ <0.6 and are mostly characterized by the absence of negative Nb–Ta and Ti anomalies, precluding a subduction-related origin.

High-field-strength element concentrations were utilized to define both a mid-oceanic ridge and seamount-type origin (Bosch et al., 2002; John et al., 2010) in medium to high P–T amphibolites and eclogites located along-strike of the Arquía Complex in southern Ecuador (the

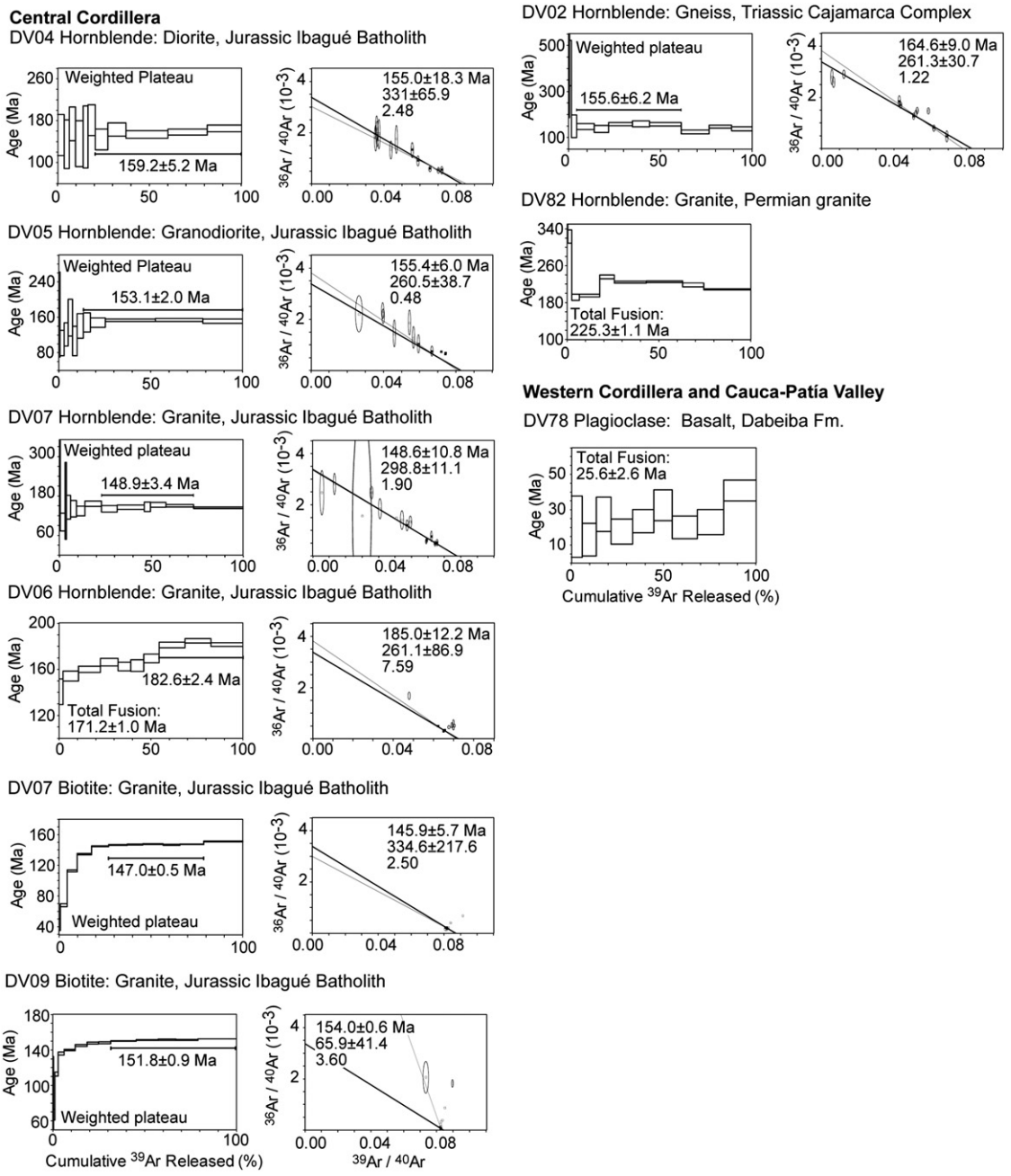

Fig. 5. $^{40}Ar/^{39}Ar$ age spectra and inverse isochron plots for hornblende, biotite and plagioclase extracted from rocks located in the Tahami Terrane (Central Cordillera) and the Chocó–Panamá Block (Western Cordillera). Inverse isochron data are presented as inverse isochron age, $^{40}Ar/^{36}Ar$ (trapped) intercept and MSWD. Plateaus are defined according to Lanphere and Dalrymple (1978). All errors are $\pm 2\sigma$.

Raspas Complex in the Amotape province, Fig. 1). The Raspas Complex lies within the same structural position as the Arquía Unit, relative to the juxtaposing Paleozoic rocks and it is likely that it is equivalent to the Arquía Complex. Tectonic discrimination based on Nb/La v $(La/Sm)_N$ (Fig. 8; after John et al., 2010) and Th v Co (Fig. 6) suggests that the protolith of the amphibolites of the Arquía Complex may also be mid-ocean ridge basalts, and also possibly hot-spot related rocks.

6.3. Allochthonous rocks of the Caribbean Large Igneous Province exposed in the Western Cordillera (Volcanic Fm.) and the Cauca–Patía Valley (Amaime Fm.)

Basalts and gabbros of the Volcanic Fm. (Western Cordillera) and Amaime Fm., (Cauca–Patía Valley; Fig. 2) show evidence of LILE remobilization due to metasomatism (locally prehnite–pumpellyite facies) but yield flat, chondrite-normalized REE patterns and a lack of negative Nb–Ta and Ti anomalies in a primitive mantle-normalized plot (Fig. 9). Samples from the Volcanic Fm. in the Western Cordillera show $(La/Sm)_N$ values of 0.95–0.68, with the exception of a single basalt (DV75; $(La/Sm)_N = 1.37$). Similarly, rocks from the Amaime Fm. yield almost identical $(La/Sm)_N$ values, with the exception of slight LREE enrichment in basalt DV112 ($(La/Sm)_N = 1.37$). Mafic rocks of the Volcanic and Amaime Fms. both plot in the ocean-plateau tholeiite field on plots of La/Yb v Zr/Th and Th v Co (Fig. 6). Finally, both formations yield Nb/Y ratios (>0.13) that are higher than those yielded by MORB rocks (Fig. 9), although they are similar to values yielded by Icelandic basalts, supporting an oceanic plateau origin for the rocks. The Amaime Fm.

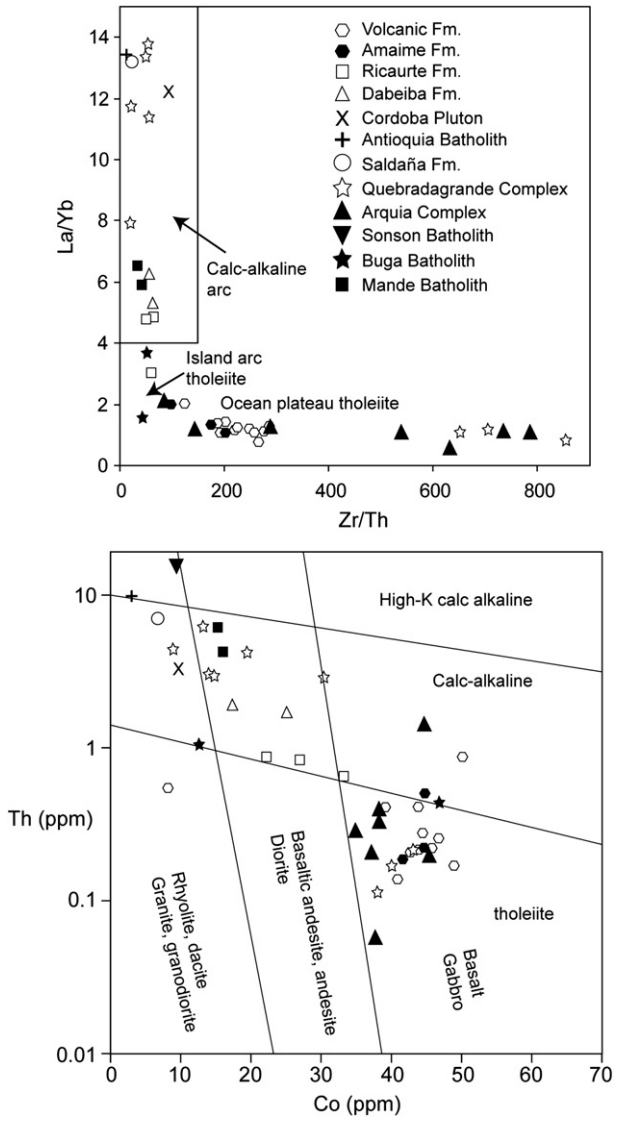

Fig. 6. La/Yb and Zr/Th tectonic discrimination (fields from Jolly et al., 2001) and Th–Co classification of igneous rocks and tectonic environments (based on Hastie et al., 2007) of rocks of the Central Cordillera, Cauca–Patia Valley and Western Cordillera of Colombia.

and Volcanic Fm. appear to be petrologically and geochemically identical.

Identical geochemical characteristics have been documented by previous studies of Western Colombia (Kerr et al., 1997, 2004) and Western Ecuador (e.g. Mamberti et al., 2003), and are typical of most of the mafic basement rocks of the Caribbean Large Igneous Province, which are considered to have erupted above a mantle plume in an oceanic environment.

6.4. Arc-related rocks within the oceanic plateau rocks

Several intermediate–acidic intrusive and volcanic rocks exposed in the Western Cordillera and the Cauca–Patía Valley yield subduction-related sequences (Figs. 6 and 9). These include the i) Late Cretaceous Buga Batholith (zircon U–Pb 92–90 Ma; Section 4.3; Fig. 2B), ii) the Mande Batholith (zircon U–Pb 43–42 Ma; Fig. 2A; Cardona, pers. comm.), which intrudes the Chocó–Panamá Terrane in the northern Western Cordillera, and iii) andesitic lavas and volcanic breccias of the Dabeiba (northern Western Cordillera; Fig. 2A) and Ricaurte Fms (southern Western Cordillera; Fig. 2C).

Primitive mantle normalized multi-element plots of these rocks yield negative Nb–Ta and Ti anomalies, and $(La/Sm)_N$ values of 2.53–1.13 (Fig. 9), which are typical of subduction zone processes. Intermediate rocks of the Mande Batholith and the Dabeiba Fm. plot within the calc-alkaline field in Co v Th and La/Yb v Zr/Th space (Fig. 6), whereas Late Cretaceous granitoids of the Buga Batholith and andesites of the Ricaurte Fm. lie on the transition between calc-alkaline and tholeiitic trends. The Buga Batholith yields a lower enrichment in LREE, with a $(La/Sm)_N$ ratio of 1.79–1.13, similar to values ($(La/Sm)_N$ ratio of 2.99–1.08) for the contemporaneous (U–Pb zircon SIMS and $^{40}Ar/^{39}Ar$ hornblende plateau age of ~90–87 Ma; Van der Lelij et al., 2010) island-arc rocks of the Aruba Batholith in the Leeward Antilles (White et al., 1999).

7. Interpretations and discussion

7.1. Pre-Early Cretaceous paleocontinental margin

Our U–Pb zircon LA–ICP–MS ages of autochthonous rocks exposed in the Central Cordillera of Colombia, show that the Tahami Terrane consists of geological units with widely varying ages that have not been properly mapped (e.g. Restrepo et al., 2009a). The oldest rocks identified within the Tahami Terrane, west of the Otú–Pericos Fault are early Paleozoic gneisses of the La Miel Unit (orthogneisses), whose protolith crystallized at a maximum time of ~440–470 Ma. These rocks were intruded by Permian granites at ~270 Ma, and all the Paleozoic sequences are unconformably overlain by Triassic metasedimentary rocks that have been partially melted and are grouped into the Cajamarca Complex.

The La Miel orthogneiss may be equivalent to lower Paleozoic granites exposed in the Santander Massif (Fig. 1) of the Eastern Cordillera of Colombia (e.g. Ocaña Batholith) (Ordóñez-Carmona et al., 2006) and various gneissic granites (Burkley, 1976) in the Mérida Andes (Fig. 1). The granitoids may represented a northward extension of Late Ordovician arc magmatism that has been documented in the Eastern Cordillera of Perú (Miskovic et al., 2009), and represent an active margin stage of the Rheic Ocean. Xenocrystic zircon U–Pb age populations within the La Miel orthogneiss cluster between 1200 and 900 Ma, indicating they were sourced from Precambrian terranes that were intruded and metamorphosed during the Grenvillian aged Sunsas Orogeny (Tassinari and Macambira, 1999). However, a paucity of zircon grains with ages that overlap the Brasiliano Orogeny (600–500 Ma; Cawood, 2005) suggests the La Miel orthogneiss may have a Laurentian basement.

Permian granites have been found along the eastern flank of the Central Cordillera (Fig. 2) and in the absence of geochemical data we propose that they form part of the metaluminous, I-type granitoid belt that is exposed in the Sierra Nevada de Santa Marta (Fig. 1; LA–ICP–MS, U–Pb zircon 288–265 Ma; Cardona et al., 2010), which probably formed via the subduction of Pacific oceanic crust beneath western Pangea. The final stages of amalgamation of Pangea took place by late Permian–Early Triassic time (Cawood and Buchan, 2007; Vinasco et al., 2006), based on geochronological data acquired from metamorphic rocks and peraluminous syntectonic intrusive rocks that formed within a collisional setting at ~250 Ma (Cardona et al., 2010; Vinasco et al., 2006).

Zircons from metasedimentary rocks of the Cajamarca Complex yield U–Pb ages characteristic of derivation from Sunsas (best exposed in eastern Bolivia) and Brasiliano mobile belts, suggesting that at least some of their source regions formed part of the cratonised region of South America (e.g. Chew et al., 2008). Precambrian and Paleozoic rocks that are now located within Central America (e.g. Chortis Block) may also represent part of the source regions and protolith for the variably foliated metasedimentary rocks of the Cajamarca Complex (240–220 Ma) that were deposited during Triassic rifting between South America and North America. The

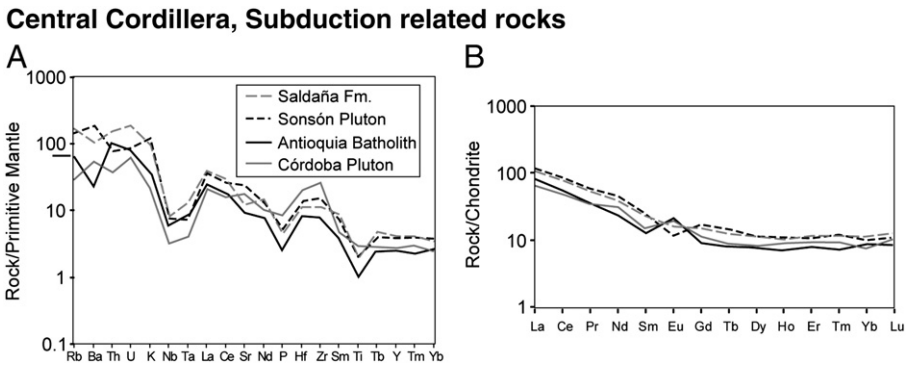

Fig. 7. Primitive-mantle-normalized trace element and C1 chondrite-normalized REE plots of samples from acidic–intermediate igneous rocks of the autochthonous Tahami Terrane in the Central Cordillera of Colombia. Normalization values are from Sun and McDonough (1989).

sedimentary sequences of the Cajamarca Fm. are temporally equivalent to Triassic syn-rift deposits observed in eastern North America, which were deposited during the fragmentation of Pangea (Pindell, 1993). Continental break-up was accompanied by high geothermal gradients and the formation of S-type granitoids (e.g. white mica-bearing granodioritic gneiss DV18; 236.2 ± 6.3 Ma) that were emplaced syntectonically within shear zones along the relict margin of South America (e.g. Tres Lagunas and Moromoro anatectites, U–Pb zircon 228 ± 3 Ma; Sabanilla Migmatite, U–Pb zircon 230 ± 3 Ma; all in Ecuador; Litherland et al., 1994; Aspden and Litherland, 1992; Chew et al., 2008). Rifting and crustal anatexis in Colombia (e.g. Vinasco et al., 2006) and Ecuador during ~240–220 Ma may have extended diachronously as far south as southern Perú, where extension-related intrusions yield Late Triassic–Early Jurassic U–Pb zircon ages of ~190–230 Ma (Miskovic et al., 2009). This event may have been responsible for thermally resetting the isotopic systems of older rocks (e.g. Permian granite DV82 yielded a $^{40}Ar/^{39}Ar$ total fusion age of 225.3 ± 1.1 Ma; Fig. 5).

The onset of subduction in Colombia and Ecuador subsequent to Triassic rifting and the opening of the western Tethys Ocean is poorly constrained (Jaillard et al., 1995). The new U–Pb and $^{40}Ar/^{39}Ar$ ages obtained from undeformed, calc-alkaline I-type granitoids of the Ibagué Batholith suggest that subduction-related magmatism was occurring along the Colombian continental margin by ~180 Ma, and probably lasted until ~147 Ma (oldest and youngest $^{40}Ar/^{39}Ar$ age obtained in this study for the Ibagué Batholith), after which a lull in magmatism commenced and the arc axis shifted oceanward at ~115 Ma (see below). A similar range of Jurassic hornblende and biotite K/Ar ages were obtained by Sillitoe et al. (1984) and Brook (1984) from the Ibagué Batholith and other small intrusive bodies. Furthermore, a similar age range has been found from the contemporary Jurassic margin of Ecuador (Chiaradia et al., 2009; Litherland et

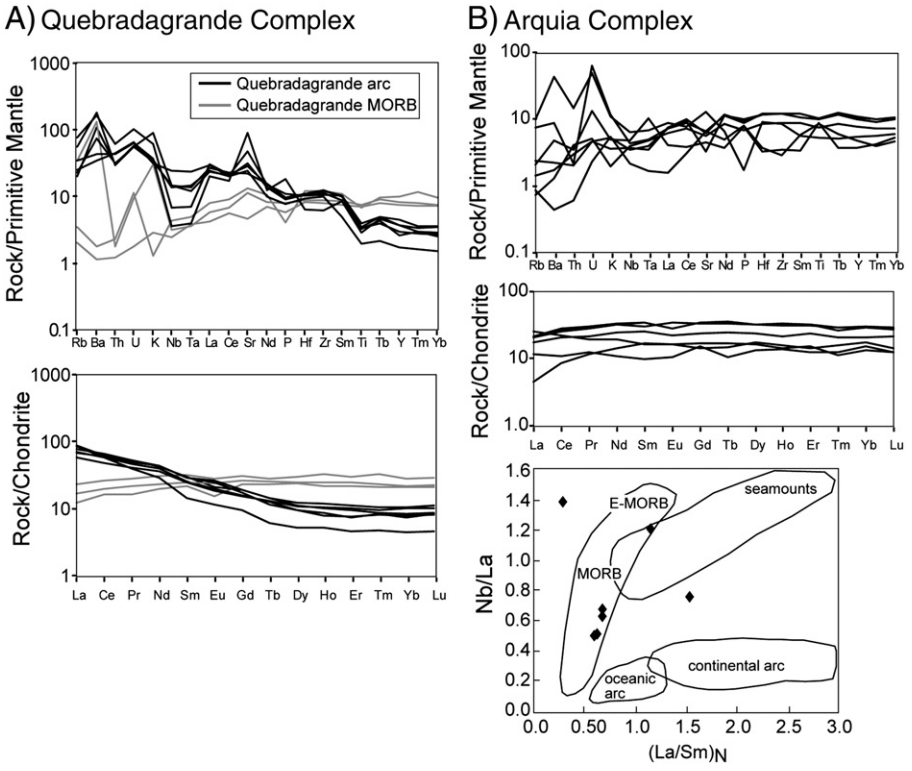

Fig. 8. Primitive-mantle-normalized trace element and C1 chondrite-normalized REE plots of mafic crystalline rocks of the Quebradagrande Complex and the Arquía Complex in the Central Cordillera of Colombia. Normalization values are from Sun and McDonough (1989). Tectonic discrimination diagram using Nb/La v $(La/Sm)_N$ is from (John et al., 2010).

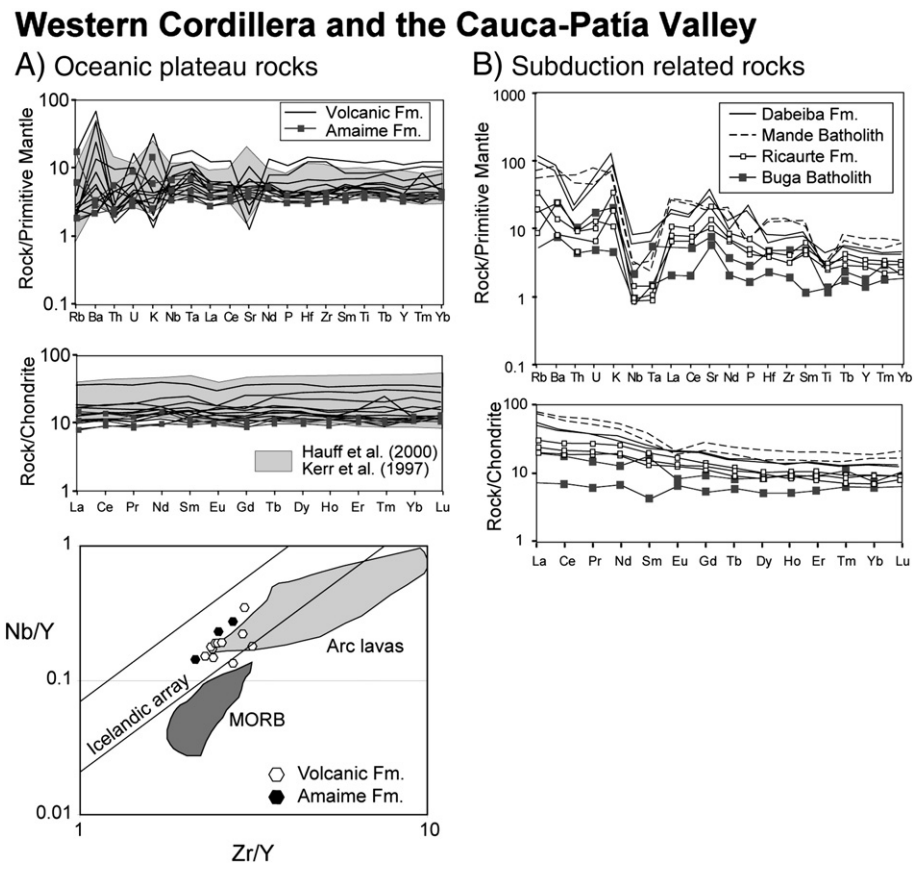

Fig. 9. Primitive-mantle-normalized trace element and C1 chondrite-normalized REE plots of the Volcanic (Western Cordillera) and Amaime Fms (Cauca–Patía Valley) of the Calima Terrane, and samples from intermediate–acidic igneous subduction-related rocks that intrude and cover the Calima terrane in Colombia. Data used from Hauff et al. (2000) and Kerr et al. (1997). Normalization values are from Sun and McDonough (1989). Tectonic discrimination based on Zr–Y v Nb–Y (Fitton et al., 1997) suggests that Volcanic and Amaime Fms. are not MORB, supporting their derivation from an oceanic plateau.

al., 1994; Spikings et al., 2001). We speculate that Jurassic continental arc magmatism ceased at ~145 Ma due to rapid, oceanward migration of the trench caused by the introduction of buoyant seamounts into the subduction system. Faulted slivers of serpentinite juxtapose the western limit of Jurassic granitoid intrusions in Colombia and Ecuador (Litherland et al., 1994). Bourgois et al. (1987) propose that the San Antonio Ophiolite Complex (Fig. 1) was obducted onto Paleozoic rocks that are currently exposed along the western flank of the Central Cordillera as early as ~140 Ma, although the ophiolitic rocks are undated. These rock sequences may represent relict components of thickened oceanic crust that hindered Late Jurassic subduction, eventually causing the trench to either migrate or jump oceanwards. Hoernle et al. (2004) report $^{40}Ar/^{39}Ar$ ages from mafic volcanic rocks of the Nicoya Peninsular (Costa Rica; Fig. 1) of 139–111 Ma, which they attribute to an oceanic plateau. The San Antonion Ophiolite may represent a relict fragment of the same plateau.

7.2. Early Cretaceous para-autochthonous terranes

Nivia et al. (2006) describe medium to high P–T rocks of the Arquía Complex as a Neoproterozoic continental block that rifted away from the continental margin, resulting in the deposition and eruption of rocks of the Quebradagrande Complex within a continental marginal basin. Their Precambrian age estimate for the protolith was based on suspect Triassic rocks that intrude the Arquía Complex, which have since been shown to be Paleocene (Restrepo et al., 2009b). Our geochemical data, combined with geochemical and isotopic data from other authors (e.g., Bustamante, 2008) suggests that the protolith of the medium to high P–T rocks of the Arquía Complex formed within a mid-ocean ridge setting, although the occasional T-MORB, chondrite-normalized signature, (Fig. 8) suggests that they may also contain components of hot-spot related material.

The Arquía Complex may be an along-strike equivalent of high-pressure rocks that are exposed in the Raspas Complex of the Amotape Province in southern Ecuador, where a MORB and seamount protolith has been proposed for eclogites and blueschists (John et al., 2010). Lu–Hf garnet ages and geobarometric studies on the Raspas Complex indicate they experienced prograde, high-pressure metamorphism at ~130 Ma at temperatures of ~600 °C (Arculus et al., 1999; John et al., 2010). The structural positions of the Raspas and Arquía complexes are extremely similar because i) both sequences are tectonically juxtaposed against an arc, and ii) both sequences are strongly foliated, and are located within the suture zone formed by the accretion of the Caribbean Large Igneous Province. Younger phengite $^{40}Ar/^{39}Ar$ ages of 129–123 Ma (Bosch et al., 2002; Gabriele, 2002) and zircon fission track ages of ~70 Ma (Spikings et al., 2005) from the Raspas Complex reflect subsequent cooling through 350–300 °C and ~250 °C, respectively. Similarly, we propose that $^{40}Ar/^{39}Ar$ ages of 117–107 Ma (Villagómez, 2010) obtained in the Arquía Complex represent cooling ages during retrogression from peak metamorphic conditions.

We propose that the Arquía Complex consists of oceanic crust that mainly formed at a mid-oceanic ridge, which was subsequently metamorphosed to high- to medium P–T conditions in an east-dipping subduction zone that gave rise to the Quebradagrande Complex. Obduction, exhumation and accretion of the Arquía Complex onto the Quebradagrande Arc and the continental margin occurred during a compressional phase during ~117 and ~107 (Fig. 10C).

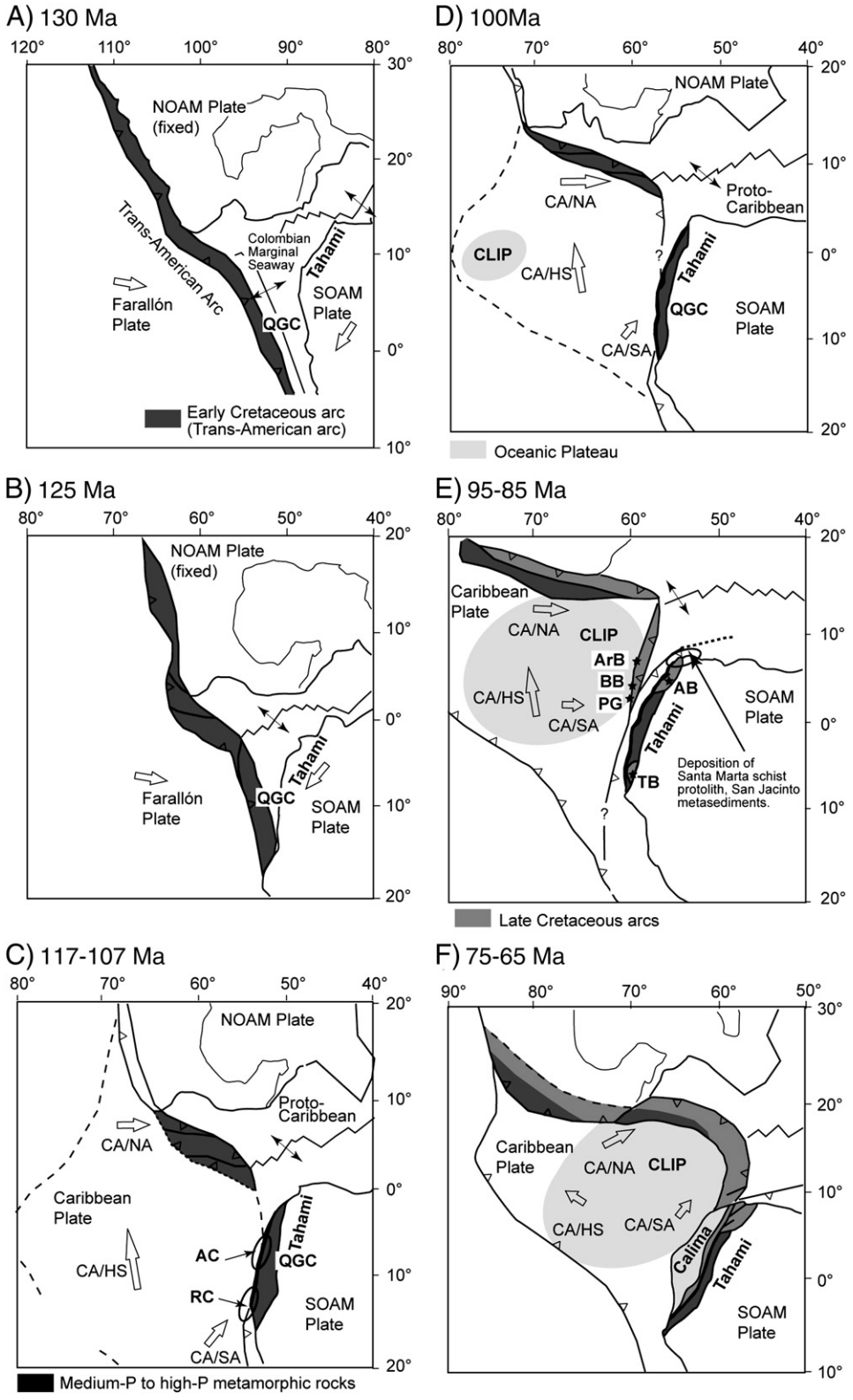

Fig. 10. Cretaceous tectonic reconstruction for northwestern South America, modified and simplified from Pindell and Kennan (2009). Relative paleopositions of North and South America from Pindell and Kennan (2009). Reference frames: A–B) North-America, C–F) Indo-Atlantic (hot spot reference frame of Müller et al., 1993). Relative convergence direction: CA/HS: Caribbean Plate/Hot spot, CA/NA: Caribbean Plate/North America, CA/SA: Caribbean Plate/South America. Abbreviations: AB: Antioquia Batholith, AC: Arquía Complex, ArB: Aruba Batholith, BB: Buga Batholith, CLIP: Caribbean Large Igneous Province, NOAM: North American Plate, PG: Pujilí Granite, QGC: Quebradagrande Complex, RC: Raspas Complex in Ecuador, SOAM: South America, TB: Tangula Batholith. The Early Cretaceous Trans-American Arc is show as dark gray, Late Cretaceous arc is shown as medium gray and the Caribbean Large Igneous Province is shown as light gray.

The Quebradagrande Complex is tectonically juxtaposed against the Arquía Complex to the west and Jurassic and older continental crust to the east, and is characterized by both MORB and Early Cretaceous (114.3 ± 3.8 Ma) arc-related rocks. Continent derived, quartz-rich sedimentary rocks within the back-arc (e.g., Abejorral Fm.; Aptian–middle Albian age; Etayo-Serna, 1985b; Toussaint, 1996) become more volcanogenic toward the arc (Gómez-Cruz et al., 1995), and cover the volcanic sequences. The arc environment was not isolated from the South American Plate although conspicuous pillow basalts and marine deposits reveal the presence of a submarine environment. Several characteristics lead us to propose that the Quebradagrande Complex erupted through oceanic or highly attenuated, transitional crust that fringed the continental margin (Fig. 10A–B). These are: i) low SiO_2 and low K arc rocks, in association with basalts with N- to T-MORB signatures, ii) most volcanic rocks erupted in submarine conditions, and sedimentary rocks were deposited in a marine setting (Etayo-Serna, 1985b; Nivia et al., 2006), and iii) the absence of continental basement to the west of the San Jerónimo fault and the lack of continent-derived detritus to the west of the volcanic rocks (Gómez-Cruz et al., 1995; Restrepo et al., 2009b). The back-arc basin is referred to here as the Colombian Marginal Seaway, so as to remain consistent with the nomenclature used by Pindell and Kennan (2009). The existence of a forearc is unclear, and may be represented by the Sabaletas Greenschist (whole rock K/Ar 127 ± 5 Ma; Toussaint et al., 1978), which displays a lower, greenschist metamorphic grade than the Arquía Complex, and had a sedimentary and mafic volcanic protolith (Garcia et al., 2007; Giraldo et al., 2007). A dramatic, oceanward shift of the arc axis from the Jurassic to the Cretaceous (Fig. 2) may have been caused by a jump in the location of the trench, driven by the accretion of buoyant oceanic crust (see Section 7.1). Amphibolites with T-MORB signatures mapped as the Arquía Fm. may be derived from the suspect buoyant indentor, and suspect ophiolites (e.g. San Antonio Ophiolite) may have obducted onto the Colombian margin in the Late Jurassic (Bourgois et al., 1987).

The Quebradagrande Complex may be coeval with the undated Alao arc of Ecuador, and the Celica–Lancones basin in southern Ecuador (Fig. 1; the Albian Alamor Fm.) (Jaillard et al., 2009).Volcanic activity toward the east of the marginal basin is recorded at least until the late Aptian (114.3 ± 3.8 Ma), which was synchronous with exhumation of the Arquía Complex during 117–107 Ma (Villagómez, 2010), indicating that the margin underwent a change from extension to compression at 120–110 Ma. We attribute the driving force of basin closure to be an acceleration of the South American Plate toward the west, as a consequence of the opening of the South Atlantic Ocean at ~120 Ma. The fate of the back-arc is unconstrained because i) the suture (San Jeronimo Fault; Fig. 2) has been reactivated, and ii) the width of the Colombian Marginal Seaway and total orthogonal displacement of the Quebradagrande Arc relative to South America is unknown. The lack of Early Cretaceous Arc rocks within the Tahami Terrane suggests that either the width of the basin was short (e.g. <100 km) or the basement to the Colombian Marginal Seaway was obducted. Late Cretaceous-Recent displacement of the entire Romeral Fault system has displaced the original rock relationships and more detailed studies are required to spatially resolve back-arc and arc components of the Quebradagrande Arc, and various components of the Arquia Complex. Perhaps the T-MORB crust of the Quebradagrande Arc formed the relict basement to the Colombian Marginal Seaway, and was originally entrained between the Arc rocks and the Tahami Terrane, although it has since been displaced.

Equivalents of the arc and T-MORB rocks mapped as the Quebradagrande Arc in the present-day southern Caribbean Realm may include metavolcanic rocks of the North Coast Schist of Tobago ($^{40}Ar/^{39}Ar$ ages >120 Ma; primitive island arc; Snoke et al., 2001; Fig. 1) and metabasalts and metagabbros (MORB; U–Pb zircon 116–109 Ma; Stockhert et al., 1995) of La Rinconada on Margarita Island, Venezuela. Primitive island arc metavolcanic rocks of the Mabujina Complex (zircon Pb–Pb >110 Ma; Grafe et al., 2001; Fig. 1), Central Cuba may be an equivalent unit that is preserved along the northern Caribbean Plate margin.

7.3. Late Cretaceous allochthonous oceanic terranes

Mafic basement rocks exposed west of the Cauca–Almaguer Fault in the Cauca–Patía Valley (Amaime Fm.) and the Western Cordillera (Volcanic Fm.; Fig. 2) share similar petrographic and geochemical characteristics (Fig. 9), consistent with them forming part of an oceanic plateau. Age data from the Palmar gabbro (zircon U–Pb 99.7 ± 1.3 Ma), Buga batholith (zircon U–Pb 92–90 Ma), which intrudes the Amaime Fm., and the Volcanic Fm. (groundmass basalt $^{40}Ar/^{39}Ar$ plateau age of 92 ± 3 Ma; Kerr et al., 1997), constrain the age of the plateau to 100–92 Ma, which overlaps with ages obtained from other regions of the Caribbean Large Igneous Province (Luzieux et al., 2006; Sinton et al., 1998; Vallejo et al., 2006), suggesting they define a single oceanic plateau sequence. The U–Pb zircon age of 99.7 ± 1.3 Ma is the oldest reliable age of the Caribbean Large Igneous Province within the northern Andes, and could be interpreted as the inception of the main phase of oceanic plateau formation (Fig. 10d).

Subduction of proto-Caribbean crust below the oceanic plateau generated an intra-oceanic arc sequence that is sporadically preserved within Colombia as the Buga Batholith (Fig. 2b) and the Espinal Fm. (U–Pb zircon 75.5 ± 1.6 Ma; Western Cordillera). The Late Cretaceous Buga Batholith (Fig. 10e) slightly predates intrusions with similar geochemical characteristics in Ecuador (Pujilí Granite; U–Pb zircon 85.5 ± 1.4 Ma; Vallejo et al., 2006) and Aruba (Aruba Batholith; ~90–87 Ma; Van der Lelij et al., 2010), both of which intrude hot-spot related mafic rocks of the Caribbean Large Igneous Province and erupted above a west-dipping subduction zone (e.g. Vallejo et al., 2009; Van der Lelij et al., 2010). The Pujilí Granite in Ecuador is considered to form part of an arc sequence that hosts volcanic rocks with $^{40}Ar/^{39}Ar$ ages of 85–72 Ma, which erupted above oceanic-plateau rocks prior to its collision with the South American Plate (Vallejo et al., 2009). The U–Pb zircon age of intercalated tuffs (75.5 ± 1.6 Ma) within the mainly sedimentary Espinal Fm. corroborates Campanian–Maastrichtian fossil ages (Etayo-Serna, 1985a), and reveals the presence of a coeval volcanic source that erupted during the waning stages of arc magmatism above a west-dipping subduction zone, prior to its collision with the continent. Given the similarities between the age and geological setting of the arc rocks within Colombia, Ecuador and Aruba, which erupted through the approaching Caribbean Plateau, we collectively refer to them as the Ecuador–Colombia–Leeward Antilles Arc (e.g. Wright and Wyld, 2011).

Late Cretaceous subduction of Proto-Caribbean oceanic crust (Fig. 10E) below the South American Plate gave rise to the continental, Antioquia and Córdoba Batholiths (U–Pb zircon 95–77 Ma; Fig. 2A–B) in Colombia. The along-strike continuity of the Late Cretaceous, continental magmatic arc toward Ecuador is uncertain, as it is only documented in southernmost Ecuador with the emplacement of the Tangula Batholith (U–Pb zircon 92.0 ± 1.0 Ma; Fig. 10e; Schütte, 2009). The northern prolongation of this subduction zone beneath northern South America may correspond to the proto-Caribbean trench (Fig. 10E) and subduction zone (Pindell et al., 1988, 2006).

Thermochronological, geochronological and sedimentological data from Ecuador shows that the Caribbean Large Igneous Province, which includes the Caribbean Plateau and its overlying arc, accreted to South America at some point between 75 and 70 Ma (Fig. 10f; Spikings et al., 2001; Vallejo et al., 2006), resulting in the cessation of east-facing arc magmatism above the section of the Caribbean Plateau that collided with the Pacific margin of Ecuador and Colombia at ~75 Ma, and the onset of rapid exhumation in the Andean cordilleras (Spikings et al., 2010). Highly deformed, syn-tectonic, Upper Cretaceous sedimentary rocks of the Nogales Fm. along the western flank of the Central

Cordillera in Colombia, and the Yunguilla Fm. along the western flank of the Eastern Cordillera of Ecuador unconformably overlie rocks of the accreted Caribbean Large Igneous Province. The suture zone is represented by the Cauca–Almaguer Fault (westernmost branch of the Romeral Fault System), which has severely dismembered the entrained rocks of the Arquía Complex and the partly overlying Nogales Fm. Collision between the Caribbean Large Igneous Province and Northern South America may have occurred diachronously, with accretionary events younging northwards along the South American margin, resulting in the collision of the Aruba Tonalite (Fig. 10E) with South America at 70–65 Ma (e.g. Van der Lelij et al., 2010).

7.4. Tertiary arc rocks in the Western Cordillera

A post-collisional calc-alkaline arc (e.g. the Paleocene Sonsón Batholith; Fig. 2B) established in the Central Cordillera of Colombia at 65–55 Ma (Ordóñez-Carmona et al., 2001). Trenchward migration of magmatism is recorded in the Paleogene with the intrusion of the Oligocene Piedrancha Pluton (K/Ar 30–23 Ma; Aspden et al., 1987) and formation of the Eocene–Oligocene Ricaurte Arc (Cediel et al., 2003) in the southern Western Cordillera (Fig. 2C). Eocene–Oligocene magmatic rocks exposed in the northern Western Cordillera of Colombia (Mande batholith and Dabeiba volcanic; Fig. 2A) may have been formed in the trailing edge of the Caribbean Large Igneous Province (Chocó–Panamá Terrane; Duque-Caro, 1990) and accreted to northwestern South America at some point between middle Miocene–early Pliocene (Cediel et al., 2003; Mann and Corrigan, 1990).

8. Conclusions

- The basement of the Central Cordillera consists of lower Paleozoic, regionally metamorphosed granitoids that are temporally correlatable with the basement of the Mérida Andes and arc rocks of the Eastern Cordillera of Perú. The granitoids may represent remnants of a Late Ordovician Arc that formed along the margins of the Rheic Ocean, and pre-date the amalgamation of Pangea. Foliated Permian granitoids probably form part of the Permian arc sequence that formed along the western margin of juxtaposing continental fragments of western Pangea.
- Triassic metasedimentary and meta-intrusive rocks within the Tahami Terrane are grouped within the Cajamarca Complex. Zircon U–Pb analyses of the metasedimentary sequence yield a maximum depositional age of ~240–220 Ma, and constrain a maximum age for high-temperature metamorphism and anatexis. Sedimentary rocks deposited during the disassembly of Pangea were accompanied by anatexis that may have diachronously propagated as far south as southern Perú.
- Continental arc magmatism commenced along the Colombian margin at ~180 Ma and lasted until ~145 Ma. The sudden termination of Jurassic magmatism may coincide with the onset of the poorly dated, Early Cretaceous Quebradagrande Arc, possibly as a consequence of the accretion of buoyant seamounts that are now preserved within the Arquía Complex and along the Nicoya Peninsular of Costa Rica. The Early Cretaceous arc is located outboard of the Jurassic arc, and erupted through either MORB of the Farallón Plate, accreted seamounts or highly attenuated transitional crust that fringed continental South America. Our interpretation is consistent with the Quebradagrande Arc forming part of the Trans-American arc of Pindell (1993).
- Medium-high P–T rocks of the Arquía Complex yield N-NORB and T-MORB characteristics, suggesting the protolith originated at a mid-oceanic ridge and may also comprise oceanic seamounts. Identical geochemical signatures yielded by high-P metamorphic rocks of the Raspas Complex (John et al., 2010) suggest they are probably along-strike equivalent rock sequences. Peak metamorphic ages of ~130 Ma (Raspas Complex) and retrogression ages (through 350–250 °C) of 117–107 Ma (Arquía Complex) suggest they represent a fragment of the subduction channel of the Quebradagrande Arc, which exhumed during ~117–107 Ma.
- Closure of the attenuated Quebradagrande Arc during ~117–107 Ma and accretion onto South America along the San Jerónimo Fault was accompanied by obduction of the Arquía Complex. Similarly, widespread Early Cretaceous exhumation of high-P rocks is observed in the forearc region of the Trans-American arc in the circum-Caribbean region (Pindell and Kennan, 2009). This phase coincides with the opening of the South Atlantic Ocean, which drove rapid westward displacement of the South American Plate.
- Geochronological and geochemical data show that the basement rocks of the Calima terrane form part of the Caribbean Large Igneous Province. Oceanic plateau rocks in Colombia range in age between 100 and 92 Ma. Mafic oceanic rocks exposed in the Cauca–Patía Valley (Amaime Fm.) and the Western Cordillera (Volcanic Fm.) form part of the same Cretaceous oceanic plateau, which is also well documented in the Western Cordillera and forearc of Ecuador.
- The remnant oceanic crust located between the converging Caribbean Large Igneous Province and South America was consumed via a divergent, double subduction system that formed an island arc through the oceanic plateau and a continental arc through northwestern South America. The island arc system includes the Buga batholith in Colombia, and probably also the Pujilí Granite in Ecuador and the Aruba Batholith in Aruba. The continental arc included the Antioquia Batholith and Córdoba pluton in Colombia.
- Collision of the Caribbean Large Igneous Province took place between 75 and 70 Ma along the Cauca–Almaguer Fault, which led to the cessation of both arcs and rapid exhumation of the paleocontinental margin (Spikings et al., 2010).
- Subduction beneath the accreted Caribbean Large Igneous Province in Colombia (Calima Terrane) resumed in the Early Tertiary, forming Paleocene arc rocks (e.g. Sonsón Batholith). Eocene arc rocks of the Dabeiba arc probably formed along the trailing edge of the Caribbean Large Igneous Province and may have collided with northwestern South America between the early Miocene–early Pliocene (Cediel et al., 2003; Mann and Corrigan, 1990).

Supplementary materials related to this article can be found online at doi:10.1016/j.lithos.2011.05.003.

Acknowledgments

Field work was supported by Andrés Mora and Luis Quiroz. The authors acknowledge the useful comments provided by James Pindell and David Chew who examined the PhD thesis of Diego Villagomez, and reviews by Iain Neill, J. Geldmacher and Andrew Kerr, which improved the content of this manuscript. This study forms part of the PhD thesis of Diego Villagómez, which was supported by funds from the Swiss National Science Foundation numbers 200021–100079 and 200021–103438.

References

Arculus, R.J., Lapierre, H., Jaillard, E., 1999. Geochemical window into subduction and accretion processes: Raspas metamorphic complex, Ecuador. Geology 27, 547–550.

Aspden, J.A., 1984. The Geology of the Western Cordillera, Department of Valle, Colombia (sheets 261, 278, 280, 299). Ingeominas-Mision Britanica (British Geological Survey), Cali-Colombia.

Aspden, J.A., Litherland, M., 1992. The geology and Mesozoic collisional history of the Cordillera Real, Ecuador. Tectonophysics 205, 187–204.

Aspden, J.A., McCourt, W.J., Brook, M., 1987. Geometrical control of subduction-related magmatism: the Mesozoic and Cenozoic plutonic history of Western Colombia. Journal of the Geological Society 144, 893–905.

Barrero, D., 1979. Geology of the Central Western Cordillera, West of Buga and Roldanillo,Colombia. Publicaciones Geológicas Especiales del Ingeominas (Bogota) 4, 1–75.

Bosch, D., Gabriele, P., Lapierre, H., Malfere, J.-L., Jaillard, E., 2002. Geodynamic significance of the Raspas Metamorphic Complex (SW Ecuador): geochemical and isotopic constraints. Tectonophysics 345, 83–102.
Bourgois, J., Toussaint, J.-F., Gonzales, H., Azema, J., Calle, B., Desmet, A., Murcia, L.A., Acevedo, A.P., Parra, E., Tournon, J., 1987. Geological history of the Cretaceous ophiolitic complexes of Northwestern South America (Colombian Andes). Tectonophysics 143, 307–327.
Brook, M., 1984. New radiometric age data from SW Colombia. Ingeominas-Mision Britanica (British Geologial Service), Colombia. report, 10.
Burkley, L. A., 1976. Geochronology of the central Venezuelan Andes. PhD thesis, Case Western Reserve University.
Bustamante, A., 2008. Geobarometria, geoquímica, geocronologia e evolução tectônica das rochas de fácies xisto azul nas áreas de Jambaló (Cauca) e Barragán (Valle del Cauca), Colômbia. PhD Thesis. Instituto de Geociências, Universidad de São Paulo, Brasil, 179.
Cardona, A., Cordani, U.G., MacDonald, W.D., 2006. Tectonic correlations of pre-Mesozoic crust from the northern termination of the Colombian Andes, Caribbean region. Journal of South American Earth Sciences 21, 337–354.
Cardona, A., Valencia, V., Garzón, A., Montes, C., Ojeda, G., Ruiz, J., Weber, M., 2010. Permian to Triassic I to S-type magmatic switch in the northeast Sierra Nevada de Santa Marta and adjacent regions, Colombian Caribbean: tectonic setting and implications within Pangea paleogeography. Journal of South American Earth Sciences 29, 772–783.
Case, J.E., Duran S, L.G., Alfonso, L.R., Moore, W.R., 1971. Tectonic investigations in Western Colombia and Eastern Panama. Geological Society of America Bulletin 82, 2685–2712.
Cawood, P.A., 2005. Terra Australis Orogen: Rodinia breakup and development of the Pacific and Iapetus margins of Gondwana during the Neoproterozoic and Paleozoic. Earth-Science Reviews 69, 249–279.
Cawood, P.A., Buchan, C., 2007. Linking accretionary orogenesis with supercontinent assembly. Earth-Science Reviews 82, 217–256.
Cediel, F., Cáceres, C., 2003. Geological Map of Colombia, GEOTEC, Ltd, Bogotá, digital format with legend and tectonostratigraphic chart. 3rd. edition.
Cediel, F., Shaw, R.P., Caceres, C., 2003. Tectonic assembly of the Northern Andean Block. In: Bartolini, C., Buffler, R.T., Blickwede, J. (Eds.), The Circum-Gulf of Mexico and the Caribbean: Hydrocarbon Habitats, Basin Formation, And Plate Tectonics: American Association of Petroleum Geologists Memoir, 79, pp. 815–848.
Chew, D.M., Magna, T., Kirkland, C.L., Miskovic, A., Cardona, A., Spikings, R., Schaltegger, U., 2008. Detrital zircon fingerprint of the Proto-Andes: evidence for a Neoproterozoic active margin? Precambrian Research 167, 186–200.
Chiaradia, M., Vallance, J., Fontboté, L., Stein, H., Schaltegger, U., Coder, J., Richards, J., Villeneuve, M., Gendall, I., 2009. U–Pb, Re–Os, and 40Ar/39Ar geochronology of the Nambija Au-skarn and Pangui porphyry Cu deposits, Ecuador: implications for the Jurassic metallogenic belt of the Northern Andes. Mineralium Deposita 44, 371–387.
Chicangana, G., 2005. Estudio del Sistema de Fallas de Romeral (0.5º–11.5º N) a partir de una caracterización sismotectónica regional. Master Thesis. Postgrado en Geología — Universidad Nacional de Bogotá, 23.
De Souza, H.A.F., Espinosa, A., Delaloye, M., 1984. K–Ar ages of basic rocks in the Patia Valley, southwest Colombia. Tectonophysics 107, 135–145.
Duque-Caro, H., 1990. The Choco Block in the northwestern corner of South America: structural, tectonostratigraphic, and paleogeographic implications. Journal of South American Earth Sciences 3, 71–84.
Etayo-Serna, F., 1985a. Trochoceramus del Campaniano-Maastrichtiano en la Formacion Espinal de la Cordillera Occidental de Colombia. Geologıa Norandina 8, 27–30.
Etayo-Serna, F., 1985b. Documentación paleontológica del Infracretácico de San Félix y Valle Alto, Cordillera Central. Proyecto Cretácico 16, 1–7.
Fitton, J.G., Saunders, A.D., Norry, M.J., Hardarson, B.S., Taylor, R.N., 1997. Thermal and chemical structure of the Iceland plume. Earth and Planetary Science Letters 153, 197–208.
Gabriele, P., 2002. HP terranes exhumation in an active margin setting: geology, petrology and geochemistry of the Raspas Complex in SW Ecuador. PhD thesis. Université de Lausanne.
Garcia, D., Vinasco, C., Weber, M., 2007. Caracterizacion de la deformacion y el metamorfismo de los esquistos de Sabaletas, parte norte de la Cordillera Central de Colombia. XI Congreso Colombiano de Geologia. 15 p.
Giraldo, M.I., Vinasco, C., Weber, M., 2007. Esquema geodinamico de la parte Noroccidental de la Cordillera Central de Colombia. XI Congreso Colombiano de Geologia. 16 p.
Gómez-Cruz, A.D.J., Moreno-Sánchez, M., Pardo, A., 1995. Edad y origen del "Complejo metasedimentario Aranzazu-Manizales" en los alrededores de Manizales (Departamento de Caldas, Colombia). Geología Colombiana 19, 83–93.
Gómez, J., Nivia, A., Montes, N.E., Jimenez, D.M., Tejada, M.L., Sepulveda, J., Osorio, J.A., Gaona, T., Diederix, H., Uribe, H., Mora, M., 2007. Geological map of Colombia. Escala 1:1'000.000. Ingeominas, 2nd Edition, Bogota.
González, H., 1980. Geología de las planchas 167 (Sonsón) y 187 (Salamina). Boletín Geológico Ingeominas 23, 174.
Grafe, F., Stanke, K.P., Baumann, A., Maresch, W.V., Hames, W.E., Grevel, Ch., Millán, G., 2001. Rb-Sr and $^{40}Ar/^{39}Ar$ mineral ages of granitoid intrusions in the Mabujina Unit, Central Cuba: thermal exhumation history of the Escambray massif. Journal of Geology 109, 615–631.
Guillong, M., Meier, D.K., Allan, M.M., Heinrich, C.A., Yardley, B.W.D., 2008. SILLS: A Matlab-Based Program for the Reduction of Laser Ablation ICP–MS Data of Homogeneous Materials and Inclusions. Mineralogical Association of Canada Short Course 40, Vancouver, B.C, pp. 328–333.
Hastie, A.R., Kerr, A.C., Pearce, J.A., Mitchell, S.F., 2007. Classification of Altered volcanic island arc rocks using immobile trace elements: development of the Th–Co discrimination diagram. Journal of Petrology 48, 2341–2357.
Hauff, F., Hoernle, K., Tilton, G., Graham, D.W., Kerr, A.C., 2000. Large volume recycling of oceanic lithosphere over short time scales: geochemical constraints from the Caribbean Large Igneous Province. Earth and Planetary Science Letters 174, 247–263.
Hoernle, K., Hauff, F., den Bogaard, Van, 2004. 70 m.y. history (139–69) for the Caribbean large igneous province. Geology 32, 697–700.
Hughes, R.A., Pilatasig, L.F., 2002. Cretaceous and Tertiary terrane accretion in the Cordillera Occidental of the Andes of Ecuador. Tectonophysics 345, 29–48.
Ibañez-Mejia, M., Tassinari, C.C.G., Jaramillo-Mejia, J.M., 2007. U–Pb zircon ages of the "Antioquian Batholith": geochronological constraints of Late Cretaceous magmatism in the Central Andes of Colombia. 11th Colombian Geological Congress, extended abstracts. 11 p.
Jaillard, E., Lapierre, H., Ordonez, M., Alava, J.T., Amortegui, A., Vanmelle, J., 2009. Accreted oceanic terranes in Ecuador: southern edge of the Caribbean Plate? Geological Society of London Special Publication 328, 469–485.
Jaillard, E., Ordoñez, M., Suárez, J., Toro, J., Iza, D., Lugo, W., 2004. Stratigraphy of the late Cretaceous–Paleogene deposits of the cordillera occidental of central ecuador: geodynamic implications. Journal of South American Earth Sciences 17, 49–58.
Jaillard, E., Sempere, T., Soler, P., Carlier, G., Marocco, R., 1995. The role of Tethys in the evolution of the Northern Andes between late Permian and late Eocene times. In: Naim, A.E.M., et al. (Ed.), The Ocean Basins and Margins. : The Tetkys Ocean, 8. Plenum Press, NewYork, pp. 463–492.
John, T., Scherer, E., Schenk, V., Herms, P., Halama, R., Garbe-Schönberg, D., 2010. Subducted seamounts in an eclogite–facies ophiolite sequence: the Andean Raspas Complex, SW Ecuador. Contributions to Mineralogy and Petrology 159, 265–284.
Jolly, W.T., Lidiak, E.G., Dickin, A.Ap., Wu, T.W., 2001. Secular geochemistry of central Puerto Rican island arc lavas: constraints on Mesozoic tectonism in the eastern Greater Antilles. Journal of Petrology 42, 2197–2214.
Kerr, A.C., Iturralde-Vinent, M.A., Saunders, A.D., Babbs, T.L., Tarney, J., 1999. A new plate tectonic model of the Caribbean: implications from a geochemical reconnaissance of Cuban Mesozoic volcanic rocks. Geological Society of America Bulletin 111, 1581–1599.
Kerr, A.C., Marriner, G.F., Tarney, J., Nivia, A., Saunders, A.D., Thirlwall, M.F., Sinton, C.W., 1997. Cretaceous basaltic terranes in Western Colombia: elemental, chronological and Sr–Nd isotopic constraints on petrogenesis. Journal of Petrology 38, 677–702.
Kerr, A.C., Tarney, J., Kempton, P.D., Pringle, M., Nivia, A., 2004. Mafic pegmatites intruding oceanic plateau gabbros and ultramafic cumulates from Bolivar, Colombia: evidence for a 'wet' mantle plume? Journal of Petrology 45, 1877–1906.
Lanphere, M.A., Dalrymple, G.B., 1978. The Use of 40ar/39ar Data in Evaluation of Disturbed K–Ar Systems. Geological Survey Open-file Report 78–701, U.S, pp. 241–243.
Litherland, M., Aspden, J.A., Jemielita, R.A., 1994. The Metamorphic Belts of Ecuador. British Geological Survey. Overseas Memoir, p. 11. doi:10.1017/S0016756897297657. 147 pp.
Ludwig, K., 2003. User's Manual for Isoplot 3.00, A geochronological Toolkit for Microsoft Excel. Berkeley Geochronology Center Special Publication, No. 4. 71 p.
Luzieux, L.D.A., Heller, F., Spikings, R., Vallejo, C.F., Winkler, W., 2006. Origin and Cretaceous tectonic history of the coastal Ecuadorian forearc between 1°N and 3°S: paleomagnetic, radiometric and fossil evidence. Earth and Planetary Science Letters 249, 400–414.
Mamberti, M., Lapierre, H., Bosch, D., Jaillard, E., Ethien, R., Hernandez, J., Polvé, M., 2003. Accreted fragments of the Late Cretaceous Caribbean–Colombian Plateau in Ecuador. Lithos 66, 173–199.
Mann, P., Corrigan, J., 1990. Model for late Neogene deformation in Panama. Geology 18, 558–562.
Marschik, R., Spikings, R., Kuşcu, I., 2008. Geochronology and stable isotope signature of alteration related to hydrothermal magnetite ores in Central Anatolia, Turkey. Mineralium Deposita 43, 111–124.
McCourt, W.J., Aspden, J.A., Brook, M., 1984. New geological and geochronological data from the Colombian Andes: continental growth by multiple accretion. Journal of the Geological Society 141, 831–845.
McDougall, I., Harrison, T., 1999. Geochronology and Thermochronology by the 40Ar/39Ar Method, 2nd ed. Oxford University Press, New York.
Miskovic, A., Spikings, R.A., Chew, D.M., Kosler, J., Ulianov, A., Schaltegger, U., 2009. Tectonomagmatic evolution of Western Amazonia: geochemical characterization and zircon U–Pb geochronologic constraints from the Peruvian Eastern Cordilleran granitoids. Geological Society of America Bulletin 121, 1298–1324.
Moreno-Sanchez, M., Pardo-Trujillo, A., 2002. Western Colombia geological history. In: Pardo, A., Moreno M, G.A. (Eds.), Stratigraphy of some Upper Cretaceous deposits of the Central and Western Cordilleras of Colombia: Regional Implications. International Journal of Tropical Geology, Geography and Ecology, pp. 91–113.
Moreno-Sanchez, M., Pardo-Trujillo, A., 2003. Stratigraphical and sedimentological constraints on Western Colombia: implications on the evolution of the Caribbean Plate. In: Bartolini, C., Buffler, R.T., Blickwede, J. (Eds.), The Circum-Gulf of Mexico and the Caribbean: Hydrocarbon Habitats, Basin Formation, and Plate Tectonics: American Association of Petroleum Geologists Memoir, 79, pp. 891–924.
Müller, R.D., Royer, J.-Y., Lawver, L.A., 1993. Revised plate motions relative to the hotspots from combined Atlantic and Indian Ocean hotspot tracks. Geology 21, 275–278.

Nivia, A., 2001. Mapa Geologico del Departamento del Valle del Cauca. Escala 1:250000. Memoria explicativa. Instituto de Investigacion e informacion geocientifica, Minero-Ambiental y Nuclear, Ingeominas, Bogota, 149 p.
Nivia, A., Marriner, G.F., Kerr, A.C., Tarney, J., 2006. The Quebradagrande Complex: a Lower Cretaceous ensialic marginal basin in the Central Cordillera of the Colombian Andes. Journal of South American Earth Sciences 21, 423–436.
Ordóñez-Carmona, O., Martins P, M., Angel, C.P., 2001. Consideraciones Geocronólogicas e Isotópicas preliminares del Magmatismo Cretáceo–Paleoceno en el norte de la Cordillera Central. In proceedings of VIII Congresso Colombiano Geologia. 5p.
Ordóñez-Carmona, O., Pimentel, M.M., 2002. Rb–Sr and Sm–Nd isotopic study of the Puquí complex, Colombian Andes. Journal of South American Earth Sciences 15, 173–182.
Ordóñez-Carmona, O., Restrepo Álvarez, J.J., Pimentel, M.M., 2006. Geochronological and isotopical review of pre-Devonian crustal basement of the Colombian Andes. Journal of South American Earth Sciences 21, 372–382.
Pindell, J., Kennan, L., 2009. Tectonic evolution of the Gulf of Mexico, Caribbean and northern South America in the mantle reference frame: an update. Geological Society of London Special Publication 328, 1–55.
Pindell, J., Kennan, L., Stanek, K.P., Maresch, W.V., Draper, G., 2006. Foundations of Gulf of Mexico and Caribbean evolution: eight controversies resolved. Geologica Acta 4, 303–341.
Pindell, J.L., 1990. Geological arguments suggesting a Pacific origin for the Caribbean Plate. In: Larue, D.K., Draper, G. (Eds.), Transactions of the 12th Caribbean Geological Conference. Miami Geological Society, St. Croix, pp. 1–4.
Pindell, J.L., 1993. Regional synopsis of Gulf of Mexico and Caribbean evolution. In: Pindell, J.L., Perkins, R.F. (Eds.), Mesozoic and Early Cenozoic Development of the Gulf of Mexico and Caribbean Region — A Context for Hydrocarbon Exploration. Foundation thirteenth annual research conference. Gulf Coast Section SEPM, pp. 251–274.
Pindell, J.L., Cande, S.C., Pitman Iii, W.C., Rowley, D.B., Dewey, J.F., Labrecque, J., Haxby, W., 1988. A plate-kinematic framework for models of Caribbean evolution. Tectonophysics 155, 121–138.
Restrepo, J.J., Dunlap, W.J., Martens, U., Ordoñez-Carmona, O., Correa, A.M., 2008. Ar–Ar Ages of Amphibolites from the Central Cordillera of Colombia and their Implications for Tectonostratigraphic Terrane Evolution in the Northwestern Andes. VI South American Symposium on Isotope Geology. Argentina. 8 p.
Restrepo, J.J., Ordoñez-Carmona, O., Martens, U., Correa, A.M., 2009a. Terrenos, Complejos y provincias en la Cordillera Central de Colombia. XII Congreso Colombiano de Geologia, 12.
Restrepo, J.J., Ordóñez-Carmona, O., Moreno-Sánchez, M., 2009b. A comment on "the Quebradagrande Complex: a lower Cretaceous ensialic marginal basin in the Central Cordillera of the Colombian Andes" by Nivia et al. Journal of South American Earth Sciences 28, 204–205.
Restrepo, J.J., Toussaint, J.F., 1976. Edades radiométricas de algunas rocas de Antioquia, Colombia. Publicacion Especial Geología. Universidad Nacional de Medellin, 12, pp. 1–11.
Restrepo, J.J., Toussaint, J.F., 1988. Terranes and continental accretion in the Colombian Andes. Episodes 7, 189–193.
Schütte, P., 2009. Geochronology, Geochemistry, and Isotopic Composition (Sr, Nd, Pb) of Tertiary Porphyry Systems in Ecuador. PhD thesis. Université de Genève, 182.
Sillitoe, R.H., Jaramillo, L., Castro, H., 1984. Geologic exploration of a molybdenum-rich porphyry copper deposit at Mocoa, Colombia. Economic Geology 79, 106–123.
Sinton, C.W., Duncan, R.A., Denyer, P., 1997. Nicoya Peninsula, Costa Rica: a single suite of Caribbean oceanic plateau magmas. Journal of Geophysical Research 102, 15507–15520.
Sinton, C.W., Duncan, R.A., Storey, M., Lewis, J., Estrada, J.J., 1998. An oceanic flood basalt province within the Caribbean plate. Earth and Planetary Science Letters 155, 221–235.
Sláma, J., Košler, J., Condon, D.J., Crowley, J.L., Gerdes, A., Hanchar, J.M., Horstwood, M.S.A., Morris, G.A., Nasdala, L., Norberg, N., Schaltegger, U., Schoene, B., Tubrett, M.N., Whitehouse, M.J., 2008. Plesovice zircon — a new natural reference material for U–Pb and Hf isotopic microanalysis. Chemical Geology 249, 1–35.
Snoke, A.W., Rowe, D.W., Yule, J.D., Wadge, G., 2001. Petrologic and structural history of Tobago, West Indies: a fragment of the accreted Mesozoic oceanic-arc of the southern Caribbean. Geological Society of America Special Paper 354, 56p.
Spikings, R.A., Crowhurst, P.V., Winkler, W., Villagomez, D., 2010. Syn- and post-accretionary cooling history of the Ecuadorian Andes constrained by their in-situ and detrital thermochronometric record. Journal of South American Earth Sciences 30, 121–133.
Spikings, R.A., Winkler, W., Hughes, R.A., Handler, R., 2005. Thermochronology of allochthonous terranes in Ecuador: unravelling the accretionary and post-accretionary history of the Northern Andes. Tectonophysics 399, 195–220.
Spikings, R.A., Winkler, W., Seward, D., Handler, R., 2001. Along-strike variations in the thermal and tectonic response of the continental Ecuadorian Andes to the collision with heterogeneous oceanic crust. Earth and Planetary Science Letters 186, 57–73.
Steiger, R.H., Jäger, E., 1977. Subcommission on geochronology: convention on the use of decay constants in geo- and cosmochronology. Earth and Planetary Science Letters 36, 359–362.
Stockhert, B., Maresch, W.V., Brix, M., Kaiser, C., Toetz, A., Kluge, R., Kruckhansleuder, G., 1995. Crustal history of Margarita Island (Venezuela) in detail: constraint on the Caribbean plate-tectonic scenario. Geology 23, 787–790.
Sun, S.S., McDonough, W.F., 1989. Chemical and Isotopic Systematics of Oceanic Basalts: Implications for Mantle Composition and Processes. Geological Society of London Special Publication 42, 313–345.
Sylvester, P.J., Ghaderi, M., 1997. Trace element analysis of scheelite by excimer laser ablation-inductively coupled plasma-mass spectrometry (ELA-ICP–MS) using a synthetic silicate glass standard. Chemical Geology 141, 49–65.
Tassinari, C.G., Macambira, M.J.B., 1999. Geochronological provinces of the Amazonian Craton. Episodes 22, 174–182.
Toussaint, J.F., 1995. Evolucion Geologica de Colombia durante el Triasico y el Jurasico. Universidad Nacional de Colombia, Sede Medellin, p. 21.
Toussaint, J.F., 1996. Evolución geológica de Colombia — Cretácico. Universidad Nacional de Colombia, Sede Medellin, p. 227.
Toussaint, J.F., Gonzalez, H., Restrepo, J., Linares, E., 1978. Edad K/Ar de tres rocas metamórficas del flanco noroccidental de la Cordillera Central. Publicación Especial Geológica Nº 14. Facultad de Ciencias, Medellín. 7 p.
Toussaint, J.F., Restrepo, J.J., 1994. The Colombian Andes during Cretaceous times. In: Salfity, J.A. (Ed.), Cretaceous Tectonics of the Andes. Verlag Braunschweig, Wiesbaden, Germany, pp. 61–100.
Vallejo, C., Spikings, R.A., Luzieux, L., Winkler, W., Chew, D., Page, L., 2006. The early interaction between the Caribbean Plateau and the NW South American Plate. Terra Nova 18, 264–269.
Vallejo, C., Winkler, W., Spikings, R.A., Luzieux, L., Heller, F., Bussy, F., 2009. Mode and timing of terrane accretion in the forearc of the Andes in Ecuador. Geological Society of America Memoir 204, 197–216.
Van der Lelij, R., Spikings, R.A., Kerr, A.C., Kounov, A., Cosca, M., Chew, D., Villagomez, D., 2010. Thermochronology and tectonics of the Leeward Antilles: evolution of the southern Caribbean Plate boundary zone. Tectonics 29, TC6003. doi:10.1029/2009tc002654.
Vesga, C., Barrero, D., 1978. Edades K/Ar en rocas ígneas y metamórficas de la Cordillera Central de Colombia y su implicación geológica. II Congreso Colombiano de Geología, Bogotá, Colombia, pp. 21–31.
Villagómez, D., 2010. Thermochronology, geochronology and geochemistry of the Western and Central cordilleras and Sierra Nevada de Santa Marta, Colombia: the tectonic evolution of NW South America., Département de Minéralogie, Université de Genève, Ph.D thesis.
Vinasco, C.J., Cordani, U.G., González, H., Weber, M., Pelaez, C., 2006. Geochronological, isotopic, and geochemical data from Permo-Triassic granitic gneisses and granitoids of the Colombian Central Andes. Journal of South American Earth Sciences 21, 355–371.
White, R.V., Tarney, J., Kerr, A.C., Saunders, A.D., Kempton, P.D., Pringle, M.S., Klaver, G.T., 1999. Modification of an oceanic plateau, Aruba, Dutch Caribbean: implications for the generation of continental crust. Lithos 46, 43–68.
Wiedenbeck, M., Allé, P., Corfu, F., Griffin, W., Meier, M., Oberli, F., von Quadt, A., Roddick, J.C., Spiegel, W., 1995. Three natural zircon standards for U–Th–Pb, Lu–Hf, trace element and REE analysis. Geostandards Newsletter 19, 1–23.
Wright, J.E., Wyld, S.J., 2011. Late Cretaceous subduction initiation on the eastern margin of the Caribbean–Colombian Oceanic Plateau: one great arc of the Caribbean (?). Geosphere 7, 468–493.